Review Article

Liyan Lai*, Yuxiao Bi, Bing Niu, Guanliang Yu, Yigui Li, Guifu Ding, and Qiu Xu

Reinforcement mechanisms and current research status of silicon carbide whisker-reinforced composites: A comprehensive review

https://doi.org/10.1515/rams-2024-0047 received November 29, 2023; accepted July 08, 2024

Abstract: In recent decades, with the advancement of micro-electro-mechanical systems technology, traditional materials have become insufficient to meet the demands of cutting-edge technology for various material properties. Composites have attracted widespread attention as an effective and viable solution. Silicon carbide whiskers (SiCw) have emerged as excellent reinforcements due to their high thermal conductivity, low thermal expansion coefficient, high melting point, superior mechanical properties, and high chemical stability. This article provides a comprehensive review of the reinforcement mechanisms and current research state of SiCw-reinforced composites. The reinforcement mechanisms include mainly grain refinement, load transfer, and crack bridging. The composites are categorized based on the type of the matrix: ceramic-based, metal-based, and polymer-based composites. The influence and parameter performance of the reinforcement mechanism on SiCw-reinforced composite materials with different matrices vary. However, the key to improving SiCw-reinforced composites lies in understanding the interplay of properties between the matrix and the reinforcement, as well as the ordered and regular distribution and binding at the interface. Finally, the current state and limitations of SiCw-reinforced composites are summarized, and future development trends are discussed. This article represents a great contribution to the future applications of SiCw-reinforced composite materials.

Keywords: silicon carbide whisker, ceramic-based composite, metal-based composite, polymer-based composite, reinforcement mechanism

1 Introduction

In recent decades, micro-electro-mechanical systems (MEMS) have emerged as a multibillion-dollar industry, encompassing various applications such as inertial sensors (accelerometers and gyroscopes), digital projectors, mechanical filters, pressure sensors, and radio-frequency resonators [1]. MEMS devices integrate mechanical and electronic components on a single chip (or equivalent structure) with high production yield and low cost, enabling the fabrication of micro-functional devices such as power generators, chemical reactors, and biomedical devices, providing unique capabilities [2].

Currently, silicon-based MEMS technology has achieved significant success in producing small-sized and usually low-cost sensor arrays used in aerospace, process control, automotive, and consumer electronics, among others [3]. However, silicon-based MEMS has certain limitations, such as being unsuitable for fabricating multi-layered MEMS devices, especially complex multi-layer movable structures. In addition, silicon is fragile at low temperatures and has poor creep strength at high temperatures, which can cause other design issues due to its properties. Therefore, it restricts the further development of MEMS devices. With the rapid advancement of MEMS, non-silicon MEMS technology has found widespread application in device fabrication [4]. Non-silicon MEMS utilizes a wide range of non-silicon materials with diverse properties. Compared to

Yuxiao Bi: School of Science, Shanghai Institute of Technology, Shanghai, 201418, China, e-mail: biyuxiao1999@163.com

Bing Niu: School of Science, Shanghai Institute of Technology, Shanghai, 201418, China, e-mail: bingniu1552@163.com

Guanliang Yu: School of Science, Shanghai Institute of Technology, Shanghai, 201418, China, e-mail: glyu@sit.edu.cn

Yigui Li: School of Science, Shanghai Institute of Technology, Shanghai, 201418, China, e-mail: ygli@sit.edu.cn

Guifu Ding: National Key Laboratory of Science and Technology on Micro/Nano Fabrication, School of Electronic Information and Electrical Engineering, Shanghai Jiao Tong University, Shanghai, 200240, China, e-mail: gfding@sjtu.edu.cn

Qiu Xu: Physical Sciences and Engineering Division, King Abdullah University of Science and Technology, Thuwal, 23955, Saudi Arabia, e-mail: xuqiulongnan@163.com

^{*} Corresponding author: Liyan Lai, School of Science, Shanghai Institute of Technology, Shanghai, 201418, China, e-mail: lailiyan312@126.com

Table 1: Characteristics of several alternatives to silicon [3]

Material name	Material characteristics			
Ceramic	Good mechanical properties, corrosion resistance, high-temperature performance			
SiC	High-temperature performance, semiconductor, excellent wear, and corrosion resistance			
Sapphire	High-temperature performance, outstanding corrosion, and wear resistance			
Quartz	Good and highly stable mechanical properties and inherent piezoelectric properties			
Polymer	Low cost and easy to manufacture			
Paper	Extremely low cost and very simple to manufacture			

silicon materials, these materials exhibit particularly attractive characteristics (Table 1), such as high-temperature performance, corrosion resistance, excellent mechanical properties, good wear resistance, and straightforward manufacturing processes. Based on the features of non-silicon microfabrication technology and the availability of various materials, versatile non-silicon MEMS devices with complex structural forms can be prepared, offering broad application prospects in aviation, aerospace, information technology, biomedicine, environment, military, and other fields [5].

As a key technology of the twenty-first century, the success of MEMS heavily relies on addressing material-related challenges associated with complex device design and fabrication [6,7]. Given the current market demand, the application of MEMS devices is expected to expand significantly, encompassing potential applications such as micro-power generation, high-frequency switches, sensors, and digital monitoring. Therefore, researchers have started exploring composites composed of two or more substances, capable of meeting specific performance requirements, to develop advanced materials with higher strength, density, electrical and thermal conductivity, dimensional stability, and microscale manufacturability [8].

Silicon carbide (SiC) has drawn extensive attention due to its low density, high strength, high melting point, excellent mechanical properties, and high chemical stability [9–11]. Its various forms, including particles, fibers, and whiskers, have shown promising results as reinforcements in composites [12–14]. Among these, SiC whiskers (SiCw) have different reinforcement mechanisms compared to SiC particles (SiCp) and exhibit excellent enhancement effects on the strength, toughness, friction, and other properties of composites. SiCwreinforced composite materials have broad development prospects due to their excellent strengthening effect.

2 SiCw-reinforced composites characteristics

2.1 SiCw characteristics

SiC is one of the most widely used ceramic materials in the industry. It possesses notable features such as high melting point, good oxidation resistance, excellent thermal conductivity, strong microwave absorption capability, wide bandgap, and high mechanical strength, making it extensively applied in aerospace, biocompatible materials, and high-temperature semiconductor devices [15,16].

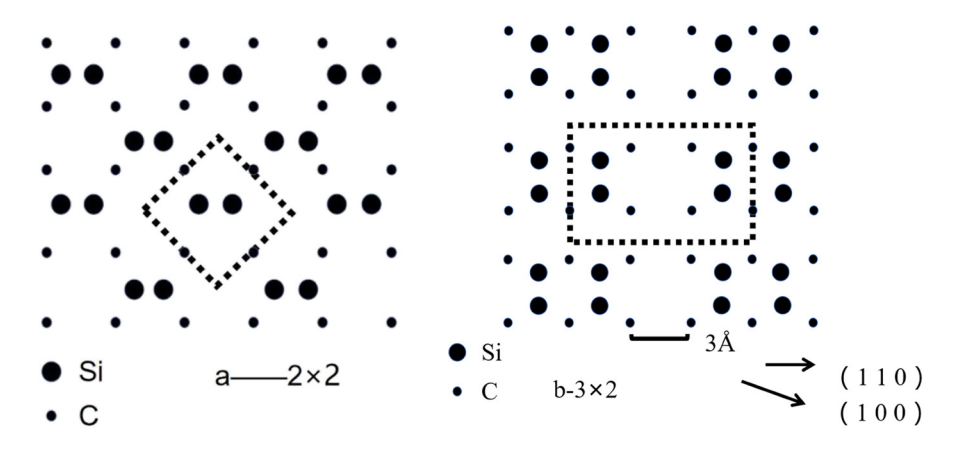


Figure 1: Crystal structure of β -SiC single crystal (001) surface [17].

SiCw is a one-dimensional nanostructured and highly ordered single-crystal SiC with a needle-like or needle-like appearance, with diameters ranging from approximately 0.1 to 5 µm and lengths exceeding 5 µm. The crystal structure of β -SiCw on the (001) surface under vacuum conditions is depicted in Figure 1. Among various structures, the C (2 \times 2) structure is more common in oxidative or neutral atmospheres, while the C (3×2) structure is more easily obtained under vacuum or reducing atmospheres. The inherent structural characteristics of SiCw result in remarkable advantages, including low density, high hardness, high elastic modulus, low thermal expansion coefficient, excellent corrosion resistance, and high-temperature oxidation resistance (Table 2). SiCw, due to its exceptional properties, has become a highly sought-after material in various industries. including electronic devices such as sensors, field emission diodes, and solar cells. Its widespread applications extend to sectors such as defense, aerospace, chemical engineering, energy, environmental protection, automotive, and many more [18-21].

2.2 SiCw composite reinforcement mechanisms

2.2.1 Mechanical properties

The reinforcement and toughening effect of SiCw on the matrix primarily depends on the interface condition between the two phases, the mechanical properties and unique structure of both the whiskers and the matrix, as well as the influence of the reinforcement on dislocation density and movement within the matrix. The strengthening mechanisms of SiCw-reinforced metal matrix composites can be classified into direct strengthening and indirect strengthening. The

former involves SiCw carrying the load and enhancing the material's performance, while the latter refers to the effect of SiCw on the matrix microstructure, including dislocations and grain size. The main strengthening mechanisms are as follows: grain refinement, Orowan strengthening, coefficient of thermal expansion (CTE) strengthening, and load transfer strengthening.

2.2.1.1 Grain refinement

The grain size of the matrix is one of the factors influencing strength. When SiCw is added to the matrix material, the whiskers act as pinning agents at the grain boundaries during the growth process of matrix grains. This effectively inhibits grain growth, leading to grain refinement and enhancing the material's ability to resist loads. This process is known as grain refinement [22-24]. The contribution of grain refinement can be calculated using the Hall-Petch formula [25-27], expressed as follows:

$$\sigma_{\rm y} = \sigma_0 + k_{\rm y} d^{-0.5},$$
 (1)

$$\Delta \sigma = k_{\rm v} (d_1^{-0.5} - d_0^{-0.5}), \tag{2}$$

where σ_y is the yield strength, σ_0 is the friction stress required for dislocation movement, k_v is the Hall-Petch constant related to the material, d is the average grain diameter, $\Delta \sigma$ represents the contribution of grain refinement to strength, and d_0 and d_1 are the average grain diameters before and after reinforcement.

It is evident that within a certain range of grain sizes, smaller grains result in higher yield strength. Therefore, the addition of a fine second phase can effectively enhance the strength of the composites. Additionally, at the same volume fraction, smaller reinforcement particles lead to better grain refinement in the composites.

Table 2: Properties of various whiskers [17]

Whisker name	Melting point (°C)	Density (g·cm ^{–3})	Tensile strength (GPa)	Specific strength (10 ⁶ cm)	Elastic modulus (GPa)	Specific elastic modulus (10 ⁶ cm)
β-SiCw	2,316	3.15	21	_	551-828	_
α-SiCw	2,316	3.15	21	_	482	_
Si ₃ N ₄	1,960	3.18	14	44	382	12
MgO	2,799	3.6	_	_	344	_
K ₂ Ti ₆ O ₁₃	1,370	3.3	6.86	_	274	_
CaSO ₄	1,450	2.96	20.5	_	178	_
BeO	2,570	2.85	13	47	350	12
B ₄ C	2,450	2.52	14	56	490	19
AIN	2,199	3.3	_	_	344	_
Al_2O_3	2,040	3.96	21	53	430	11

2.2.1.2 Orowan strengthening

Orowan strengthening is a mechanism in which the interaction between dislocations and second-phase particles leads to an increase in strength. When dislocations encounter the reinforcement particles, they bypass and form dislocation loops, creating obstacles to dislocation movement and inducing hardening [28]. The formation of dislocation loops increases the lattice distortion energy, thereby increasing the resistance to dislocation movement [29]. The Orowan reinforcement theory formula is

$$\tau_{\rm c} = \tau_{\rm m} + \frac{T}{bl/2},$$

where $\tau_{\rm c}$ is the shear strength of composite materials, $\tau_{\rm m}$ is the shear strength of the matrix, b is the Burgers vector of the matrix, l is the average spacing of reinforcements, and T is the dislocation line tension. The premise of Orowan strengthening is that the strength of the reinforcement phase is sufficient to resist dislocation motion. SiCw, with its high strength, meets the requirements for strengthening, but its high aspect ratio makes it challenging to form dislocation loops [30,31]. As a result, SiCw-reinforced composites can experience Orowan strengthening, but this mechanism typically does not dominate.

2.2.1.3 Thermal mismatch strengthening

When the matrix and reinforcement phase are well bonded at the interface in the composites and have a significant difference in the CTE, the production process induces lattice distortion near the interface, increasing the resistance to dislocation migration toward the grain boundary and thus enhancing the material's strength [32]. This strengthening mechanism is known as thermal mismatch strengthening, also known as CTE strengthening. The strengthening effect of CTE in the composites can be expressed by the following formula [33]:

$$\Delta \sigma_{\rm CTE} = \alpha G b \sqrt{\rho}$$
, (3)

where $\Delta\sigma_{\text{CTE}}$ is the increment in CTE strengthening, α is the material constant, G is the shear modulus of the matrix, b is the Burgers vector of the matrix, and ρ is the dislocation density.

Arsenault and Shi [34] studied the increase in dislocation density caused by thermal mismatch in composite materials using *in situ* transmission electron microscopy and established a relevant model:

$$\Delta \rho = \frac{\Delta \alpha \Delta TNA}{b},$$

where $\Delta \rho$ is the increase in dislocation density, $\Delta \alpha$ is the difference in CTE between reinforcement and matrix, ΔT is

the temperature difference, N is the number of reinforcements, A is the total surface area of each reinforcement, and b is the Burgers vector of the matrix. According to the above formula, the effect of thermal mismatch strengthening decreases with the increase of the size of the reinforcement and increases with the increase of the volume fraction of the reinforcement.

2.2.1.4 Load transfer strengthening

Load transfer strengthening involves transferring external loads through the interface to the main carrying phase (whiskers). The theory is based on the shear-lag model [35,36], assuming that SiCw is oriented in the direction of the applied load. The strengthening effect of load transfer on the performance of composite materials mainly depends on the interface strength between the reinforcement and the matrix, as well as the volume fraction and aspect ratio of the reinforcement. Kelly and Tyson [37] revised the shear lag model, which is the most commonly used description of the load transfer mechanism:

$$\sigma_{\rm c} = \sigma_{\rm m} \left[\frac{V_{\rm w}(s_{\rm w} + 2)}{2} + V_{\rm m} \right],$$

where σ_c is the yield strength of composite materials, σ_m is the yield strength of the matrix, V_w is the volume fraction of whiskers, s_w is the whisker aspect ratio, and V_m is the volume fraction of the matrix.

When the average length of the whiskers is less than the critical length at which they can bear the maximum stress within the matrix, failure occurs through debonding and pullout. Conversely, when the whisker length exceeds the critical length, failure occurs through fracture [38–40]. The load transfer strengthening formulas are as follows [41,42]:

$$\Delta \sigma_{\rm LT} = \sigma_{\rm r} V_{\rm r} \left(\frac{L}{2L_{\rm c}} \right) - \sigma_{\rm m} V_{\rm r}, \quad (L < L_{\rm c}), \tag{4}$$

$$\Delta \sigma_{\rm LT} = \sigma_{\rm r} V_{\rm r} \left(1 - \frac{L}{2L_{\rm c}} \right) - \sigma_{\rm m} V_{\rm r}, \quad (L \ge L_{\rm c}), \tag{5}$$

$$L_{\rm c} = \frac{d\sigma_{\rm r}}{2\tau_{\rm m}},\tag{6}$$

where $\Delta\sigma_{\rm LT}$ represents the increment in load transfer strengthening; $\sigma_{\rm r}, V_{\rm r}, L$, and $L_{\rm c}$ refer to the strength, volume fraction, average length, and critical length of the reinforcement phase (whiskers), respectively; $\sigma_{\rm m}$ is the strength of the matrix; and $\tau_{\rm m}$ is the tensile strength of the matrix.

Fracture mechanics theory indicates that the essence of material toughness lies in the properties of crack propagation. From an energy balance perspective, the critical condition for crack propagation in a solid is when the elastic strain energy release rate equals the fracture energy required per unit area of crack extension. Therefore, any factors affecting this balance can modify the material's toughness. The reinforcement effect of whiskers on the matrix depends significantly on the interface condition between the two phases. A favorable interface bonding state facilitates the effective utilization of whiskers, leading to superior performance. Several mechanisms contribute to the enhancement of fracture toughness ($K_{\rm IC}$) in whisker-reinforced composites, and they are as follows [43–45]:

(a) Crack bridging

When a crack propagates to the whisker, a bridging zone is formed at the crack tip. The whisker bridges the crack, applying compressive stress on the crack surfaces, reducing the force acting on the crack tip, and suppressing further crack extension, thereby enhancing toughness. As the load increases, the whisker eventually fractures or pulls out, allowing the crack to continue to propagate, thus significantly consuming fracture energy [46,47], as shown in Figure 2.

(b) Crack deflection

When the crack propagates to the whisker, it must either deviate around or pass through the whisker to continue its propagation. When the crack surface makes a small or even parallel angle with the whisker orientation, the crack will tend to propagate along the whisker direction due to the strong bonding between the whisker and the matrix. This leads to a change in the crack propagation direction, causing the crack's path to lengthen and the newly generated crack surface area to increase. As a result, the material absorbs more energy during the fracture process, leading to an improvement in material toughness [47,49], as illustrated in Figure 3.

(c) Pull-out effect

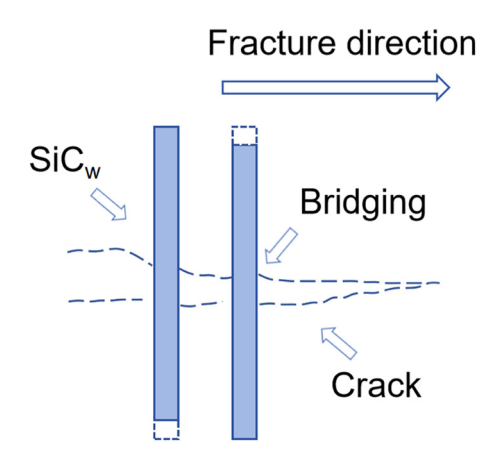


Figure 2: Schematic of crack bridging [48].

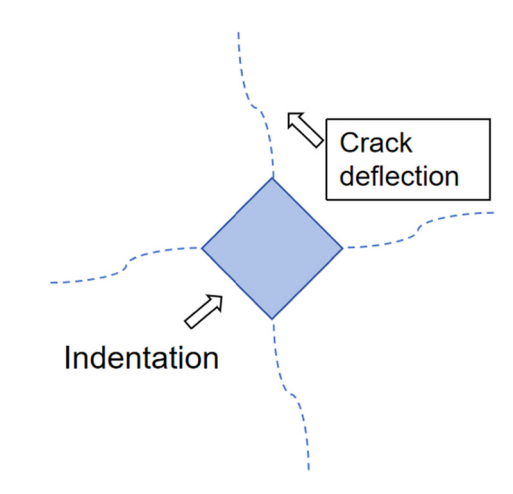


Figure 3: Schematic diagram of crack deflection [48].

When the whisker orientation forms a large angle with the crack surface, the shear stress generated at the interface between the matrix and the whisker reaches the shear yield strength of the matrix but not that of the whisker. As a result, the whisker consumes additional energy to overcome the interfacial bonding and pulls out from the matrix, a phenomenon known as the pull-out effect. Under certain conditions, a longer pull-out length corresponds to a greater energy consumption, leading to a more significant enhancement of the whisker-reinforced material. Therefore, comparing the pull-out lengths of whiskers can serve as an indirect method to assess the effectiveness and utilization of the whisker reinforcement [50].

It is obvious that the prerequisite for whisker pull-out is whisker debonding, which requires energy to generate a new interface. Assuming that the debonding energy of the whiskers is equal to the strain release energy on the whiskers caused by stress release, the debonding energy of each whisker is

$$\Delta Q = (\pi d^2 \sigma_{\rm w}^2 l_{\rm c})/48 E_{\rm w},$$

where ΔQ is the whisker debonding energy, d is the whisker diameter, $\sigma_{\rm w}$ is the whisker strength, $l_{\rm c}$ is the whisker pull-out length, and $E_{\rm w}$ is the whisker modulus. After the whisker debonding, the whisker pull-out relaxes the stress at the crack tip, slowing down the propagation of cracks and improving the toughness of the composite material [51].

The interface bonding between the whisker and the matrix can be classified into two types: physical bonding and chemical bonding. When the interface is physically bonded, the two phases are mechanically interlocked with a relatively low interface bonding strength. In this case, the pull-out effect primarily occurs due to the overcoming of frictional forces [52]. Conversely, when the interface is

chemically bonded, a new phase is formed at the interface, and the two phases are joined by chemical bonds, resulting in a higher interface bonding strength. This situation reduces the likelihood of interface debonding and whisker pull-out, which is beneficial for strengthening and toughening the composite. However, if the interface bonding is excessively strong, surpassing the whisker strength, the interface debonding and whisker pull-out may not occur, leading to whisker fracture instead [53,54]. By appropriately reducing the interface bonding strength, the pull-out effect of the whisker can be fully utilized to enhance the strength and toughness of the composites [55].

2.2.2 Frictional performance

Friction inevitably leads to wear, which characterizes the continuous damage of the surface materials in mutual contact during relative motion. Materials separate from the surface in the form of particles or flakes. This separation process in materials causes the formation and propagation of cracks until detachment from the matrix. From this perspective, wear is a mechanism of surface damage caused by mechanical forces. Generally, wear can be classified into four basic types: abrasive wear, adhesive wear, surface fatigue wear, and corrosive wear [56].

2.2.2.1 Abrasive wear

When external hard particles or asperities on the sliding surface act on the material surface during friction, material is detached from the surface due to the action of these abrasive particles, which is called abrasive wear. The force of abrasive particles on the solid surface can be divided into two components: the normal force and the tangential force. The normal force presses the abrasive particles into the material surface, while the tangential force propels the abrasive particles forward. When the shape and orientation of the abrasive particles are appropriate, they act like cutting tools, creating chips on the material surface.

2.2.2.2 Adhesive wear

Adhesive wear occurs when two materials in relative motion adhere to each other due to the welding or adhesion between the two sliding surfaces. In this wear mechanism, material is detached and adheres to the opposing surface, resulting in the formation of wear debris during friction.

2.2.2.3 Surface fatigue wear

In rolling or sliding with rolling friction and sliding friction, cyclically changing contact stresses cause fatigue spalling of the material, leading to the formation of pits. This type of wear is referred to as surface fatigue wear or contact fatigue wear. Factors influencing fatigue wear include material properties, contact stress, and physical and chemical characteristics of the contact surfaces.

2.2.2.4 Corrosive wear

Corrosive wear refers to the phenomenon where material undergoes environmental chemical or electrochemical reactions with the surrounding medium during friction, resulting in a reduction or transfer of the surface material. Chemical reactions and mechanical actions may occur either simultaneously or subsequently. For instance, chemical reactions may happen first, followed by the removal of corrosion products through mechanical action, or the generation of small fragments may precede environmental reactions. Even slight chemical reactions can enhance the effects of mechanical action.

The wear mechanisms vary for different materials, but usually, one mechanism dominates, while sometimes multiple mechanisms coexist. In SiCw-reinforced composites, the wear mechanism in frictional behavior changes with the effectiveness of SiCw reinforcement. When the matrix material is in its inherent state, it is influenced by its intrinsic strength. A matrix with lower intrinsic strength is more prone to adhesion, resulting in higher wear rates due to matrix transfer. Therefore, the wear mechanism in this case is generally dominated by adhesive wear [57,58]. When the content of the reinforcing phase is relatively low, the introduction of the second phase leads to the exposure of detached whiskers during friction. These detached whiskers become abrasive particles that contribute to the wear process in addition to adhesive wear. Hence, the wear mechanism becomes a combination of adhesive wear and abrasive wear [59,60]. As SiCw content increases, the strength of the material also increases gradually. The increased strength reduces the occurrence of adhesive wear, and the higher SiCw content enhances whisker agglomeration, resulting in increased porosity of the composites. Consequently, during wear, whiskers are more likely to detach and join the wear process as abrasive particles, leading to abrasive wear becoming dominant with the increase in the content of the reinforcing phase [61–63]. When the strength of SiCw composites is enhanced to a certain extent, minimal deformation occurs during friction, and no significant damage is visible. However, after extended periods of friction, under repeated cyclic stresses, the region just beneath the material surface becomes the primary site for energy accumulation and dissipation, causing thermal aging, chemical degradation, or other effects that reduce the material strength. As a result, the wear mechanism transitions from adhesive wear to fatigue wear [64,65].

For particle-reinforced composites, whiskers generally show better enhancement in the material's frictional performance, and the unique properties of whiskers such as orientation and aspect ratio significantly influence the frictional behavior.

SiCw acts as hard phases in wear, protecting the matrix and bearing the load [66]. When the whiskers are oriented perpendicular to the friction surface, they are deeply embedded in the matrix, preventing plastic deformation along the sliding direction of the surface. According to the delamination theory, cracks parallel to the friction surface are less likely to initiate and propagate perpendicular to the whiskers, resulting in reduced whisker detachment. Consequently, there are few whiskers in the wear debris, and the wear surface does not exhibit deep plowing. However, when the whiskers are oriented parallel to the friction surface, the material's resistance to plastic deformation is poorer, and cracks are more likely to propagate along the axial direction of the whiskers, leading to increased detachment of whiskers in the wear particles.

2.2.3 Thermal properties

The thermal conductivity of composites is related to the inherent thermal conductivity of the reinforcing and matrix materials, as well as the type, size, and content of the reinforcing phase [67,68]. Due to its large aspect ratio, good thermal conductivity, and excellent physical properties such as mechanical strength and stiffness, SiCw are considered effective reinforcing agents for thermally conductive composites [69–71]. For matrix materials with low thermal conductivity, the addition of SiCw can effectively improve the thermal conductivity of the composite. For other matrix composites, the addition of whiskers is more critical for improving other properties.

When the content of the reinforcing phase is low, SiCw is surrounded by the matrix and has little interaction with each other. At this stage, the interaction between whiskers is weak, and no thermal pathway or network is formed inside the composites. Thus, the thermal conductivity of the composites increases slowly with the increase in the content of the reinforcing phase [72]. Under high content of the reinforcing phase, SiCw with a high aspect ratio tends to contact with each other, forming thermal pathways or networks, providing a pathway for phonon transmission.

Therefore, the thermal conductivity of SiCw-reinforced composites increases rapidly, and the relationship between thermal conductivity and the content of the reinforcing phase exhibits nonlinearity [73–75].

The thermal conductivity of composites mainly depends on the thermal pathways or networks inside the material. For matrix materials with low thermal conductivity, high content of the reinforcing phase can result in higher thermal conductivity [76]. However, a high content of SiCw may introduce defects and voids into the composites, which not only reduces the mechanical properties but also leads to a large interfacial thermal resistance, thus reducing the thermal conductivity of the composite [77,78]. Therefore, to obtain composites with high thermal conductivity and good mechanical properties, it is necessary to select an appropriate content of the reinforcing phase and take effective measures to optimize the interface. Surface modification of the reinforcing phase is one of the effective measures to improve interface compatibility and enhance the interaction between the reinforcing phase and the matrix [79,80].

The academic community has proposed many theoretical and empirical models to predict the effective thermal conductivity of composites [81–85]. For SiCw-reinforced composites, the simplest approach is to consider the reinforcing and matrix materials as being parallel or series arranged in terms of heat flow. This method can calculate the upper or lower limit of the effective thermal conductivity. For parallel conduction models:

$$K_{\rm c} = K_{\rm m} V_{\rm m} + K_{\rm r} V_{\rm r}. \tag{7}$$

For the series conduction model:

$$K_{\rm c} = \frac{V_{\rm m}}{K_{\rm m}} + \frac{V_{\rm r}}{K_{\rm r}},\tag{8}$$

where K_c is the thermal conductivity of the composites, K_m and V_m are the thermal conductivity and volume fraction of the matrix material, respectively, and K_r and V_r are the thermal conductivity and volume fraction of the reinforcement material.

Maxwell utilized the potential theory to derive a model for the thermal conductivity of uniform spheres with a random distribution and no mutual interaction within a homogeneous medium. However, to account for the influence of reinforcement particle shapes on the thermal conductivity of composites, modifications to the Maxwell equation are considered, as follows [86]:

$$K_{\rm c} = K_{\rm m} \frac{\left[K_{\rm r} + (n-1)K_{\rm m} + (n-1)V_{\rm r}(K_{\rm r} - K_{\rm m})\right]}{\left[K_{\rm r} + (n-1)K_{\rm m} - V_{\rm r}(K_{\rm r} - K_{\rm m})\right]}, \quad (9)$$

where n is the shape factor related to the sphericity of the reinforcement. If the reinforcement has a spherical shape,

n = 3, and the equation can be simplified to the original Maxwell equation. However, SiCw has a high aspect ratio, which results in n > 3.

The Agari model, as a semi-theoretical model for predicting the thermal conductivity of polymer composites, introduces two factors, C_1 and C_2 , to consider the influence of the filler's dispersion state in the matrix. This is in contrast to previous models [87]:

$$\log K_{\rm c} = V_{\rm r} C_2 \log K_{\rm r} + (1 - V_{\rm r}) \log(C_1 K_{\rm m}), \tag{10}$$

where C_1 is a factor related to crystallinity and crystal size, while C_2 indicates the ability to form thermal conductivity chains in the filler. According to the Agari model, the value of C_2 largely depends on the filler's capability to form thermal conductivity chains, with $0 < C_2 < 1$. Due to SiCw's higher aspect ratio compared to SiCp, SiCw have a C_2 value closer to 1, making them more prone to form thermal conductivity chains and networks [88].

2.2.4 Dielectric properties

Traditional dielectric materials, such as organic polymers and inorganic ceramics, are no longer able to meet the strict requirements of advanced capacitors. Additionally, efficient dissipation of the heat generated by electronic devices to maintain their working temperature at the desired level is crucial. This is because the dielectric strength of dielectric materials decreases with increasing temperature due to their poor thermal conductivity [89,90]. Therefore, SiCw with high dielectric performance and high thermal conductivity has become an excellent reinforcement for dielectric composites, as its excellent heat dissipation capability helps extend the lifespan of the dielectric material under higher working temperatures [91].

Polarization is an inherent property of dielectric materials, referring to the generation of dipoles and migration of positive and negative charges in the material under an external electric field, resulting in an electric dipole moment. According to the polarization mechanisms inside dielectric materials, polarization types can be categorized into four types (Figures 4 and 5) [92–94]:

- (1) Electronic polarization: In an applied electric field, the positive atomic nuclei and negative electrons experience relative displacement, creating a net dipole moment known as electronic polarization. Electronic polarization occurs in the frequency range of 10¹⁴–10¹⁶ Hz and is independent of temperature changes for any material under an applied electric field.
- (2) Ionic polarization: Ionic crystals consist of positive and negative ions held together by ionic bonds. In the absence of an electric field, the positive and negative ions are aligned, resulting in electrical neutrality. However, in the presence of an external electric field, the positive and negative ions undergo relative displacement, generating an electric dipole moment

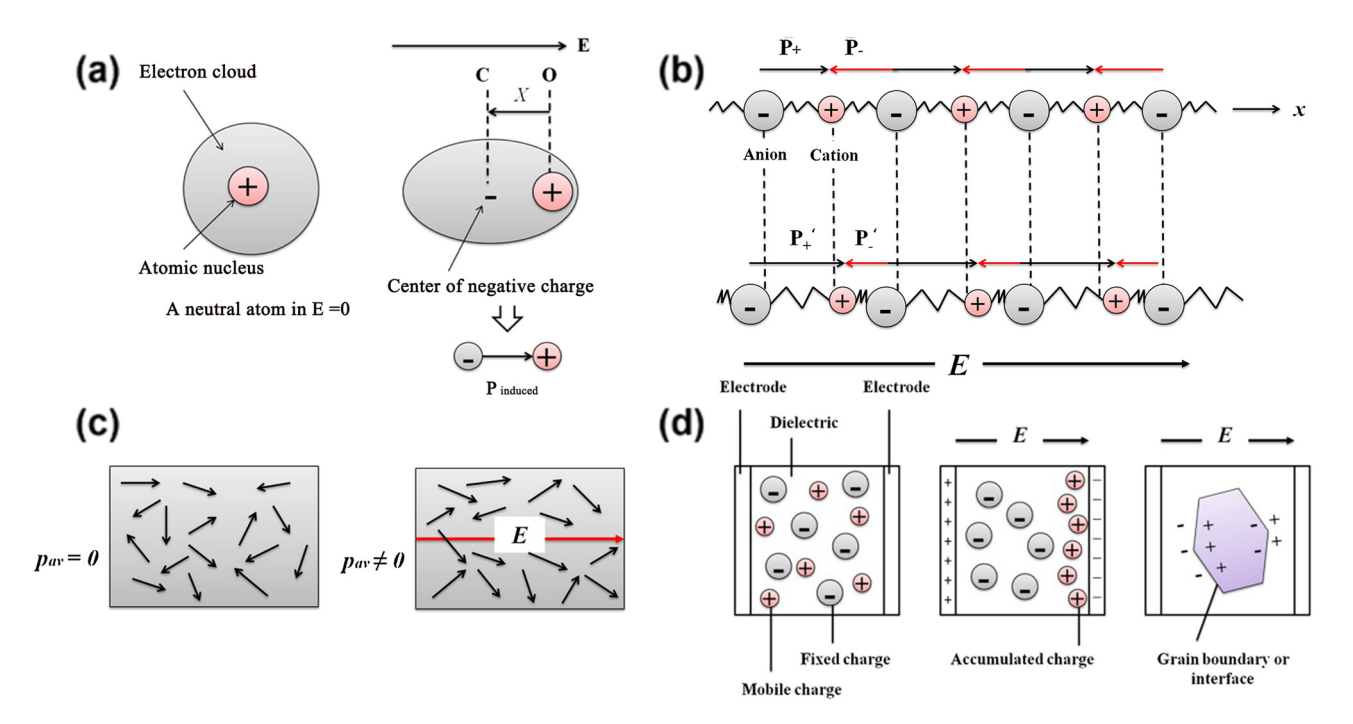


Figure 4: Four polarization forms: (a) electron polarization, (b) ionic polarization, (c) dipole polarization, and (d) interface polarization.

known as ionic polarization. Ionic polarization occurs in the frequency range of 10^9 – 10^{13} Hz.

- (3) Orientation polarization (dipole polarization): Orientation polarization typically occurs in molecules with permanent dipole moments. In the absence of an electric field, the dipole moments of molecules are randomly arranged, resulting in a total dipole moment of zero, making the molecules electrically neutral. However, under the influence of an external electric field, the dipole moments of molecules align in an ordered manner along the direction of the electric field, resulting in a non-zero total dipole moment known as orientation polarization. Orientation polarization occurs in the frequency range of 10³–10⁸ Hz and exhibits a strong temperature dependence.
- (4) Interface polarization (IP, space charge polarization): Interface polarization usually occurs at the interfaces between two or more phases of composites. Due to the presence of phase interfaces in composites, charge carriers migrate to the interface, where they get trapped by defects. Under the influence of an external electric field, the trapped charge carriers undergo separation, resulting in a dipole moment known as interface polarization. Since the formation of space charge takes time, interface polarization occurs in the frequency range of 10⁻²–10³ Hz and only affects the dielectric performance of materials under direct current and low-frequency conditions.

SiCw has dimensions at the micro and nanometer levels, and smaller dimensions result in a larger interface area, which promotes interface polarization in dielectric composites [95]. Based on the doping of the reinforcement, dielectric composites can be classified into two categories [96]: dielectric—dielectric nanocomposites containing semi-conducting nanofillers with high dielectric constants and dielectric-conductive nanocomposites containing conductive nanofillers.

For dielectric-conductive nanocomposites, the dielectric constant ε can be described using the following model [97,98]:

$$\varepsilon = \varepsilon_{\rm m} |V - V_{\rm c}|^{-S}, \tag{11}$$

where $\varepsilon_{\rm m}$ is the dielectric constant of the matrix, V is the volume fraction of the reinforcement, s is an exponent close to 1, and $V_{\rm c}$ is the percolation threshold of the reinforcement.

In SiCw-reinforced dielectric composites, due to the higher electrical conductivity of semiconductor SiCw compared to the matrix, charge carriers at SiCw-matrix interface act as electron dipoles, enhancing the polarization effect of the composites. At low SiCw content ($V < V_c$), the dielectric constant shows slight frequency dependence. As SiCw whiskers are well-isolated, charge separation is significantly restricted, resulting in lower electron polarization, and the dielectric constant increases linearly and slowly with SiCw concentration [99,100]. When SiCw content approaches the percolation threshold, the dielectric constant increases sharply, indicating the onset of percolation. When electrons can tunnel or hop between several adjacent conductive particles, the charge confined within individual filler particles can be significantly released, enhancing charge separation and leading to a rapid increase in the dielectric constant. At higher SiCw content ($V > V_c$), as SiCw

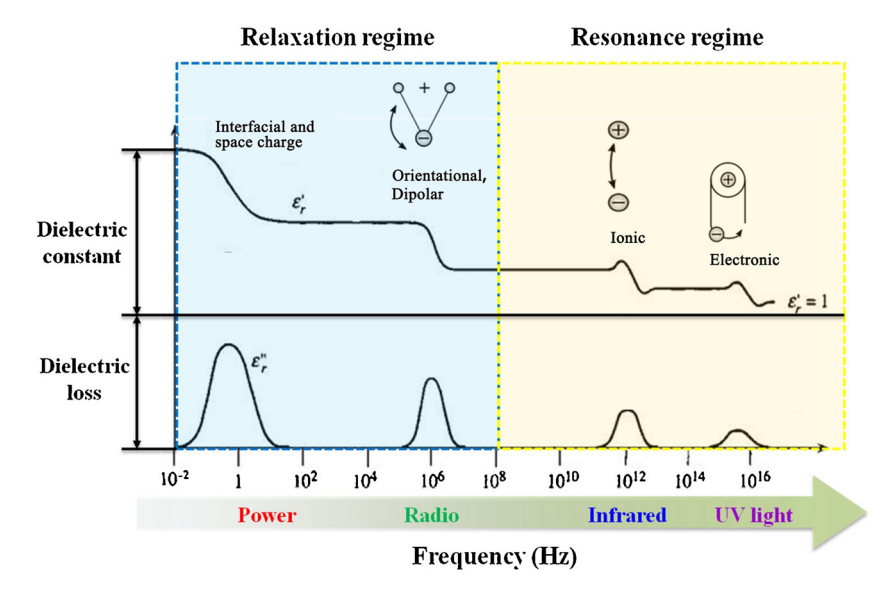


Figure 5: Four polarization types and their frequency dependence.

whiskers come into contact with each other, long-range charge carrier migration occurs [101]. In this case, the dielectric constant shows a decrease over a wide frequency range, and a strong frequency dependence is observed. Unlike the good frequency stability at lower content, strong frequency dependence signifies strong interface polarization, also known as the Maxwell–Wagner–Sillars effect, occurring in non-uniform phases with different conductivities, leading to an enhanced dielectric constant [102–104].

The essence of the percolation threshold model transition is when the volume fraction V of the reinforcement increases to the critical (percolation) threshold V_c , the reinforcements start to establish extensive contact with each other, forming a conductive network that spans the entire system. Before the conductive network is fully connected $(V < V_c)$, the separated reinforcements act like micro-capacitors. As the volume fraction approaches the critical value, each micro-capacitor exhibits an abnormally large capacitance. This process promotes the migration and accumulation of charge carriers at the interface between the polymer and conductive filler. These charge carriers are generated either by surface plasmon resonance or by charge injection from external electrodes. This charge accumulation continues as the frequency increases until the percolation transition occurs, during which the distance between adjacent conductive fillers becomes lower than the electron tunneling range or direct contact. During the charge accumulation process, the carriers at the interface enhance interface polarization, leading to a significant increase in dielectric constant at lower frequencies.

For SiCw-reinforced composites, dielectric loss (ε'') can be described using the following model [105]:

$$\varepsilon'' = \varepsilon_{\rm dc}'' + \varepsilon_{\rm MW}'' + \varepsilon_{\rm D}'', \tag{12}$$

where ε_{dc}'' is the conduction loss factor, ε_{MW}'' is the interface polarization loss factor, and ε_{D}'' represents the dipole loss factor.

The conduction loss factor is obtained from the following equation:

$$\varepsilon_{\rm dc}'' = \frac{\sigma_{\rm dc}}{2\pi f},\tag{13}$$

where σ_{dc} and f represent the direct current conductivity and frequency, respectively.

Usually, dielectric loss can be regarded as the sum of polarization loss and leakage loss in the studied frequency range. The composites exhibits an initial decrease and subsequent increase as the frequency increases. The low-frequency dielectric response is believed to originate from IP and leakage [106–108]. IP mainly results from charge

carriers trapped at the interface between the reinforcement and the matrix, while SiCw contributes more significantly to leakage. At low SiCw content ($V < V_c$), the dielectric loss of the composites is nearly independent of the whisker content, mainly due to the larger distance between the reinforcements [109–111]. At high SiCw content ($V > V_c$), the dielectric loss of SiCw-reinforced dielectric composites first increases sharply to a very high level and then decreases rapidly with increasing frequency. The high dielectric loss at low frequencies results from the direct current conduction of the conductive network formed by high-content SiCw, leading to charge accumulation at the phase interfaces and during the electron conduction process [112]. Therefore, for SiCw-reinforced dielectric composites, high dielectric loss with strong frequency dependence is often observed.

In further optimizing the performance of SiCw-reinforced dielectric composites, constructing a core–shell structure for the fillers is considered the most effective method to suppress dielectric loss. By coating the surface of SiCw with organic or inorganic insulating layers, the dramatic increase in dielectric loss and leakage current at $V_{\rm c}$ can be significantly suppressed to a low level [106].

3 SiCw-reinforced composites

SiCw was initially developed in the early 1960s, but its application was initially limited to reinforcing metal matrices such as aluminum. These metal-matrix composites were only a minor commercial success, mainly due to the high cost of SiCw, which made it prohibitively expensive. It was not until the 1980s that whisker-reinforced ceramic materials (alumina) were first prepared. From then on, people began to develop industrial-scale methods for mass-producing whiskers at an acceptable cost. Today, SiCw has become an economically viable reinforcement material and has been applied in electronic devices such as sensors, field emission diodes, and solar cells [113]. With the rapid development of composites and the successful commercialization of some products, the demand for whiskers has also increased. Over the years, many companies have developed various methods for growing whiskers and have filed multiple patents in this field. Currently, commercially available whiskers are limited to a few companies, with SiCw being the main focus. Additionally, these companies have also researched and produced TiC, TiN, Al₂O₃, mullite, Si₃N₄, and B₄C whiskers. However, SiCw remains the most studied and commercially successful whisker [114,115].

DE GRUYTER

Keinforcement	Matrix	Special process	Whisker loading	Whisker loading Density (g·cm ⁻³) Properties	Properties	Ref.
SiCw	(Hf–Ta–Zr–Nb–Ti)C	High-energy ball milling, spark plasma sintering	5 wt%	99.4%	$K_{\rm IC} = 3.14 \pm 0.15$; $E = 461.2 \pm 5.4$	[125]
SiCw	SIAICN	Mechanical alloying, spark plasma sintering	5 wt%	3.02	$\sigma_{\rm f} = 523.2 \pm 14.1$; HV = 19.6 \pm 0.6	[126]
PyC-SiCw	RBSC	Reaction sintering process, CVD	10 wt%	I	$\sigma_{\rm f} = 510$; $K_{\rm IC} = 5.28$	[127]
SiCw	Al_2O_3	3D printing technology	10 vol%	97.1%	$\sigma_{\rm f} = 405 \pm 98$; $K_{\rm IC} = 7.1 \pm 1.20$; HV = 17.6 ± 0.84	[128]
SiCw	Sioc	3D printing technology	5 wt%	1.77	$\sigma_{\rm c} = 98.4 \pm 12.3$	[129]
SiCw	$ZrO_2-AI_2O_3$	Oscillatory pressure sintering	15 vol%	I	$\sigma_{\rm f} = 461$; $K_{\rm IC} = 6.97 \pm 0.13$; HV = 13.01	[130]
SiCw	SIAICN	Mechanical alloying, spark plasma sintering	5 wt%	ı	$K_{IC} = 5.8$; $\sigma_f = 523.2$	[48]
SiCw	SiC	Vat photopolymerization, liquid silicon infiltration	8 wt%	2.95	$\sigma_{\rm f} = 352.2$; HV = 17.54	[131]
SiCw	Sico	Digital light processing	5 wt%	I	$\sigma_{\rm f} = 260.1 \pm 49.7$; $K_{\rm IC} = 3.23 \pm 0.12$	[132]
SiCw	SiC	Oscillatory pressure sintering	5.42 wt%	99.45%	HV = 30.68 ; $K_{IC} = 6.66$; $\sigma_f = 733$	[133]

 χ_c : Fracture toughness (MPa·m^{-1/2}); σ_i : Flexural strength (MPa); σ_c : Compressive strength (MPa); HV: Hardness (GPa); E: Young's modulus (GPa).

3.1 SiCw-reinforced ceramic-based composites

Ceramic materials are typical brittle materials and very sensitive to structural defects, and their low $K_{\rm IC}$ greatly limits their application range. To overcome the drawbacks of low $K_{\rm IC}$ and high defect sensitivity in ceramic materials, various ceramic-based composites reinforced with particles [116,117], whiskers [118–120], and continuous fibers [121–123] have been developed and extensively studied. These composites are commonly used in the manufacturing of components for aerospace vehicles, gas turbines, and other related applications [124].

Compared to single-base materials, SiCw-reinforced ceramic-based composites exhibit significantly improved mechanical properties and have potential application value. Adding SiCw to ceramic materials can enhance their strength, $K_{\rm IC}$, thermal conductivity, thermal shock resistance, and high-temperature creep performance. These discoveries have sparked further research into these composites.

Table 3 shows the current progress of SiCw reinforced ceramic matrix composites. Tiegs [134] analyzed the toughening behavior of SiCw-reinforced alumina composites and found that crack—whisker interactions, including crack bridging, whisker pull-out, and crack deflection, are the main toughening mechanisms. For these mechanisms to be effective, debonding along the alumina matrix—whisker interface (usually associated with crack deflection) must occur during crack propagation, allowing the whiskers to bridge the crack at their tails. Observations of the fracture surfaces of whisker-reinforced composites revealed rough fracture surfaces with clearly visible whiskers under a microscope, as shown in Figures 6 and 7.



Figure 6: Fracture surface of SiCw-reinforced alumina showing very rough surface and tortuous crack propagation [134].

12 — Liyan Lai et al. DE GRUYTER

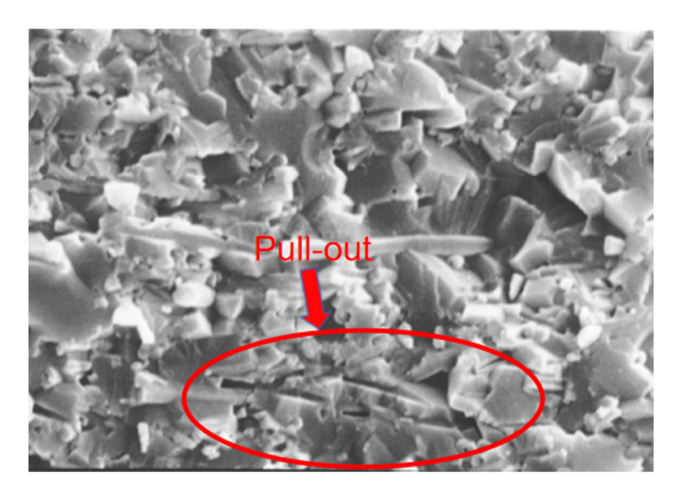
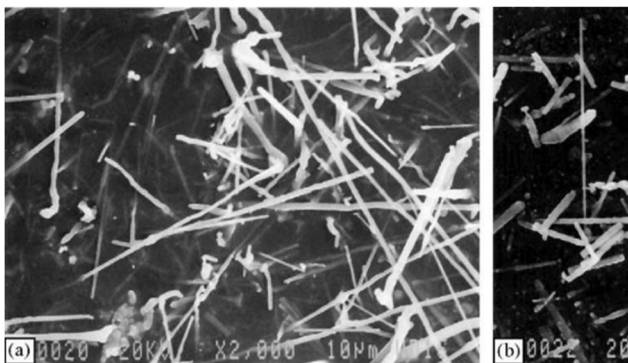


Figure 7: Fracture surface of SiCw-reinforced alumina. SiCw is clearly observed on the exposed surfaces [134].

Garnier *et al.* [135] studied the thermodynamic properties of SiCw-reinforced Al₂O₃-based composites with two different surface chemical compositions, where SiCw content was 35 vol%. The two types of whiskers had different oxygen contents, with low oxygen content (6 at%) and high oxygen content (39 at%), labeled as "L" and "H," respectively (Figure 8). Whisker "L" had a smaller cross-sectional area, while whisker "H" had a relatively larger cross-sectional area and surface roughness. They separately mixed

the two types of whiskers with Al₂O₃ to form slurries and then fabricated the composites using hot-pressing at 45 MPa. 1,850°C, and in a nitrogen environment. The study revealed that the surface chemical composition of the whiskers was related to the thermomechanical properties of the composites, primarily influenced by the oxygen content on their surfaces. High oxygen content on the whisker's surface affected the interface bonding between the whiskers and the matrix. The test results of the mechanical properties at room temperature are shown in Table 4. Additionally, the authors investigated the influence of the two types of whiskers on the mechanical properties of the composites in the range of 800-1,300°C (Figure 9). After high-temperature heat treatment of SiCw-reinforced Al₂O₃-based composites, SiCw underwent oxidation in an air environment, leading to the formation of an amorphous substance. The amorphous softening occurred above 1,200°C, indicating that the oxygen content on the surface of SiCw raw material also significantly influenced the high-temperature mechanical properties of the composites.

SiCw-reinforced alumina-based composites have shown significant improvements in mechanical properties, such as strength and $K_{\rm IC}$. These composites are typically densified through pressure-assisted sintering, specifically hot pressing, with SiCw content ranging from 10 to 30 vol%. They are mainly applied in the field of high-nickel alloy cutting tools,



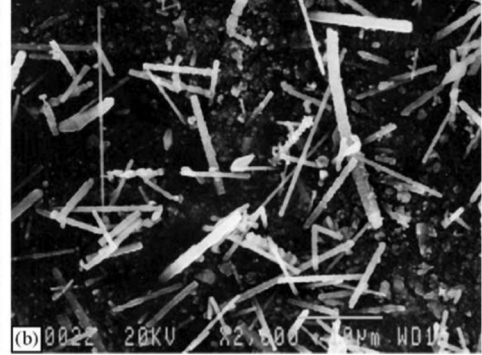


Figure 8: SEM micrographs of SiCw: (a) "L" whisker and (b) "H" whisker [135].

Table 4: Room temperature mechanical properties of Al₂O₃–35 vol% SiCw "L" and "H" composites [135]

Mechanical properties	Al ₂ O ₃	Al ₂ O ₃ + 35 vol% SiCw "L"	Al ₂ O ₃ + 35 vol% SiCw "H"
Relative density (dth%)	99.1	100	99.6
Young's modulus (GPa)	406 ± 10	421 ± 10	407 ± 9
Vickers hardness (10 kg)	1,854 ± 38	2,107 ± 32	2,032 ± 62
Flexural strength (MPa)	488 ± 151	639 ± 21	549 ± 41
$K_{\rm IC}$ (MPa·m ^{-0.5})	5.4 ± 0.4	7.9 ± 0.3	6.9 ± 0.2

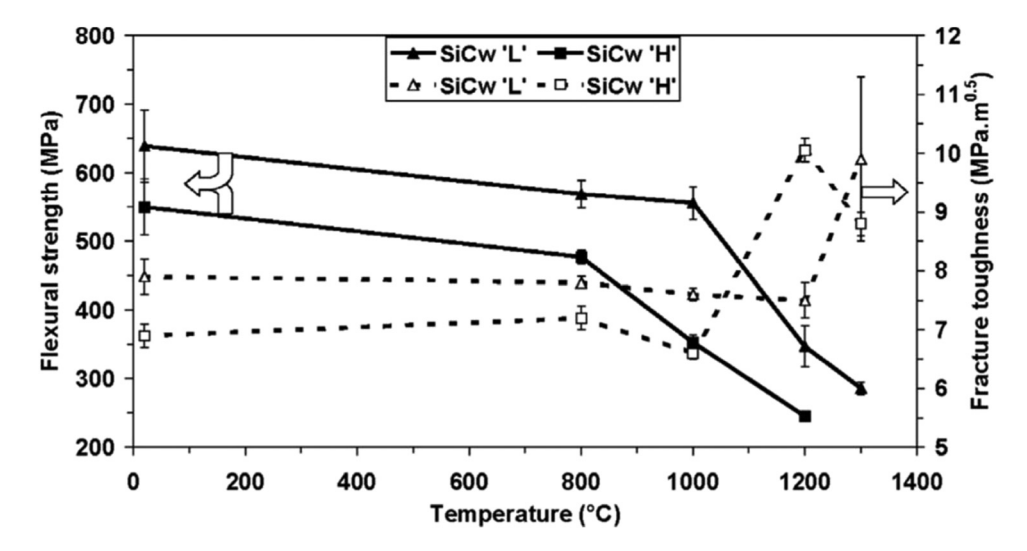


Figure 9: Variation of flexural strength and K_{IC} with temperature [135].

while their applications in other wear-resistant and structural fields are still under development.

Song *et al.* [136] reported on SiCw-reinforced composites with SiCp as the matrix material, prepared using a reactive sintering method at 1,650°C. They investigated the effect of KH-550 pre-treatment on the dispersion performance of SiCw and its subsequent influence on the mechanical properties of the composites. The study examined the variation of mechanical properties with different SiCw contents (0–20 wt%). The results showed that the mechanical properties of SiCw were significantly improved after KH-550 pre-treatment (Table 5). The composites reached its maximum flexural strength and $K_{\rm IC}$ at a SiCw content of 15 wt% (290 MPa and 5.6 MPa·m^{-1/2}, respectively, Figure 10).

Chen et al. [137] employed a gel-casting combined with precursor infiltration and pyrolysis (PIP) method to prepare SiCw-reinforced SiCp composites. They investigated the influence of different SiCw volume fractions on the microstructure and mechanical properties of SiCw/SiC composites, and further explored the enhancement mechanism. The results showed that as the volume fraction of whiskers increased from 34.81 to 41.9%, the flexural strength and $K_{\rm IC}$ of the composite exhibited a trend of rapid enhancement followed by a gradual increase. When the volume fraction reached 41.9%, both the flexural strength and $K_{\rm IC}$ reached

their maximum values of $308.2 \,\mathrm{MPa}$ and $5.32 \,\mathrm{MPa} \cdot \mathrm{m}^{-1/2}$, respectively (Figure 11).

Wu *et al.* [138] fabricated SiCw-reinforced Ti (C, N) based composites using the vacuum sintering method. They investigated the influence of different whisker contents on transverse rupture strength (TRS), $K_{\rm IC}$, and hardness (HRA), and analyzed the underlying mechanisms. The experimental results showed that the particle size of the composites was related to the amount of SiCw added. When SiCw content was 1.0 wt%, the composites exhibited the smallest particle size, and their mechanical properties were in the optimum state, with TRS and $K_{\rm IC}$ values reaching as high as 2,279 MPa and 17.7 MPa·m $^{-1/2}$, respectively (Figure 12). However, when SiCw content was further increased to 2.5 wt%, the porosity in the composites increased, and some whiskers agglomerated, leading to a decline in the mechanical properties of the composites.

Zhou *et al.* [139] used a vacuum hot-pressing sintering technique to prepare MoSi₂/SiCw reinforced Si₃N₄-based composite ceramic cutting tool materials at 1,650°C. They investigated the influence of different reinforcement phase contents on the microstructure, mechanical properties, and friction and wear performance of the composites, and analyzed the underlying mechanisms. The experimental results showed that with the increase of SiCw

Table 5: Room temperature mechanical properties of the composites [136]

Materials	Flexural strength (MPa)	K _{IC} (MPa·m ^{-1/2})
15 wt% SiCw (as-received)	256 ± 11	3.4 ± 0.08
15 wt% SiCw (pre-coated)	290 ± 12	5.6 ± 0.1

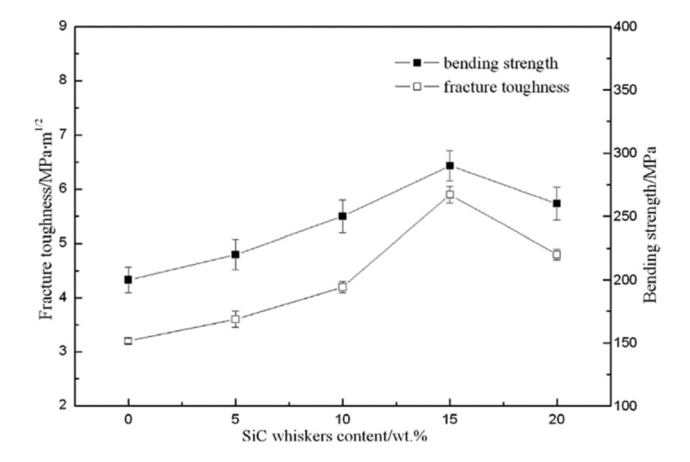


Figure 10: Variation of flexural strength and K_{IC} of pre-coated SiCw-RBSC ceramics with mass fractions from 0 to 20 wt% [136].

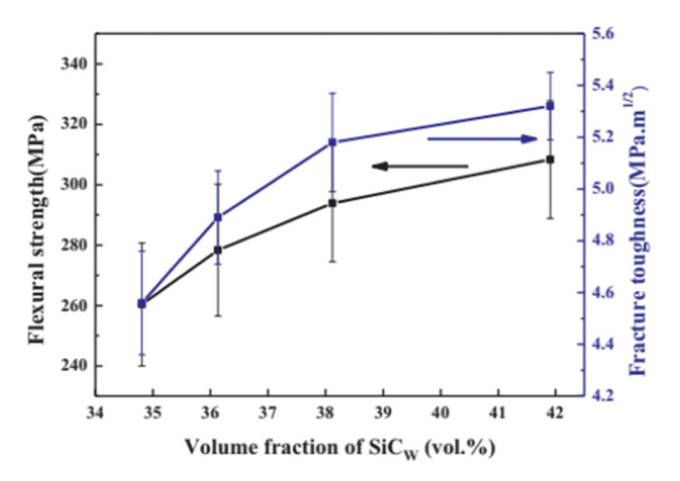


Figure 11: Flexural strength and K_{IC} of SiCw/SiC composites with different SiCw volume fractions [137].

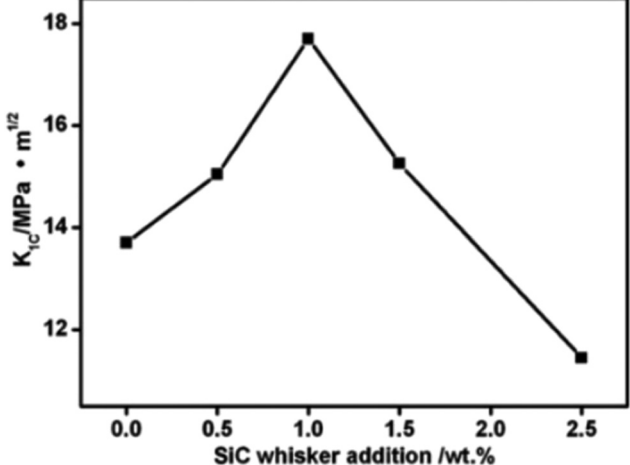


Figure 12: Effects of SiCw on K_{IC} of Ti (C, N)-based metal cermets [138].

content as the reinforcing phase, $K_{\rm IC}$ of the ceramic cutting tool material continuously increased, and the anti-wear capability significantly improved. The wear mechanism transitioned gradually from adhesive—abrasive composite wear to abrasive wear. The weight loss and wear depth of the composites decreased significantly (Figures 13 and 14), indicating that the addition of SiCw effectively enhanced the wear resistance of $\rm Si_3N_4$ ceramics. When the MoSi₂ and SiCw contents were both 10 wt%, the grain size was smaller, and the material exhibited higher density, enhancing the bridging and pull-out effects of whiskers. Therefore, the material showed better mechanical properties, with a flexural strength of 888.21 MPa, $K_{\rm IC}$ of 10.22 MPa·m^{-1/2}, and HRA of 19.17 GPa.

The strength and toughness of the above-mentioned SiCw-reinforced ceramic-based composites can be enhanced to a certain extent. The degree of enhancement depends not only on the preparation conditions of the composites (such

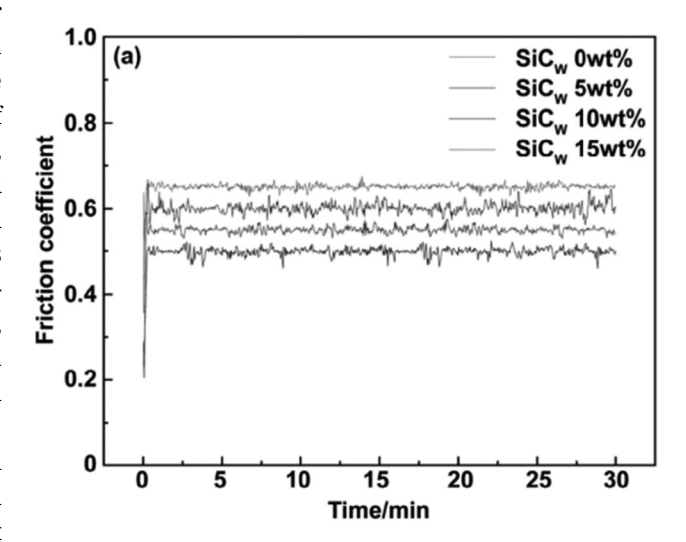


Figure 13: Effects of SiCw addition friction coefficient [139].

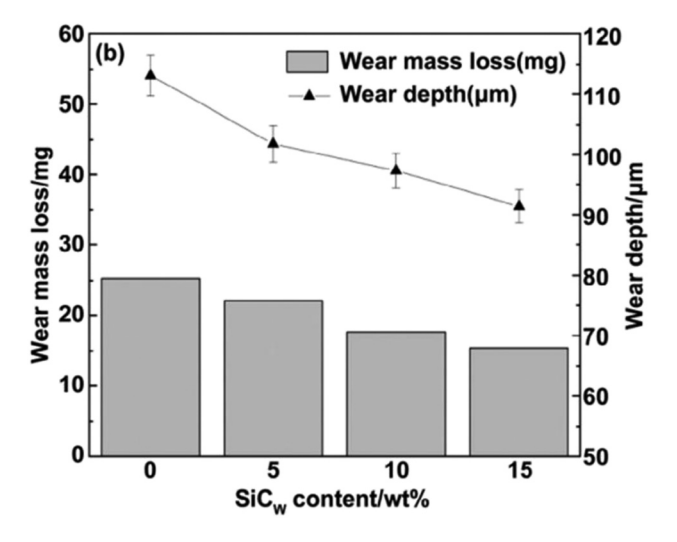


Figure 14: Effects of SiCw addition on wear weight loss and wear depth [139].

as temperature, pressure, binder, and pH value of the slurry) but also largely on the content of SiCw added to the composites. Currently, SiCw-reinforced ceramic-based composites have been successfully applied in the cutting tools, engine structural components, and heat exchanger linings, among other applications. Below are listed some mechanical properties of SiCw-reinforced ceramic-based composites at room temperature, as shown in Table 6.

Based on existing experimental data and micromechanical models, the toughness $K_{\rm IC(composite)}$ of the composite can be described as the sum of the toughness of the matrix $K_{\rm IC(matrix)}$ and the toughening contributed by the whiskers $K_{\rm IC(whisker-reinforced\ phase)}$, as expressed by Eq. (14) [134]:

$$K_{\rm IC(composite)} = K_{\rm IC(matrix)} + K_{\rm IC(whisker-reinforced phase)}$$
. (14)

Table 6: Mechanical properties of SiCw toughened and reinforced ceramics [140]

Composites	Strength (MPa)	Toughness (MPa·m ^{-1/2})
Al_2O_3	500	4
$Al_2O_3 + SiCw (20 vol\%)$	800	8.7
$Al_2O_3 + ZrO_2$ (15 vol%)	1,080	6.2
$Al_2O_3 + ZrO_2$ (15 vol%) +	1,100-1,400	6–8
SiCw (15 vol%)		
Mullite	244	2.8
Mullite + SiCw (20 vol%)	452	4.4
$3Y - TZP (+3 wt\% Y_2O_3)$	1,150	6.8
3Y - TZP + SiCw	590-610	10.2-11.0
(20-30 wt%)		
Si_3N_4	520	5.14
Si ₃ N ₄ + SiC (20 vol%)	890	11.3

There are two associated whisker toughening mechanisms [141,142], represented by Eqs. (15) and (16):

$$\Delta K_{IC}(W \cdot R) = \sigma_{f} \cdot \sqrt{\frac{V_{f} \cdot r}{B \cdot (1 - v^{2})} \cdot \frac{E_{c}}{E_{\omega}} \cdot \frac{V_{m}}{V_{i}}}, \qquad (15)$$

where $\Delta K_{\rm IC}(W\cdot R)$ is the toughness improvement due to whisker reinforcement, $\sigma_{\rm f}$ is the fracture strength of the whisker, $V_{\rm f}$ is the volume fraction of whiskers in the composite, r is the radius of the whisker, v is Poisson's ratios of the whisker and the composite, $E_{\rm c}$ and $E_{\rm \omega}$ are Young's moduli of the composite and the whisker, respectively, $y_{\rm m}$ and $y_{\rm i}$ are the fracture energies at the whisker bridging and at the interface between the matrix and the whisker, and B is a constant that depends on the stress distribution at the bridging site.

$$\Delta K_{IC}(W \cdot R) = f dS^2 / E + 4L_i f(d/R) / (1 - f), \tag{16}$$

where $\Delta K_{\rm IC}(W\cdot R)$ is the toughness improvement due to whisker reinforcement, f is the volume fraction of whiskers, d is the length of debonding of the whiskers, S is the length of the whiskers, E is Young's modulus of the whiskers, and E is the diameter of the whiskers.

From the analysis and discussion of toughening mechanisms and the two toughening behaviors mentioned above, it is evident that the toughening of whisker-reinforced composites depends on parameters such as whisker diameter, strength, volume fraction, as well as the elastic moduli of the matrix and the whiskers, and the interfacial fracture energy between them [143–145]. The whisker's characteristics, such as diameter, strength, and surface chemistry, directly influence the toughening mechanisms and mechanical behavior, while the surface chemistry affects the interface bonding between the whisker and the matrix [146].

3.2 SiCw-reinforced metal matrix composites

SiCw-reinforced metal matrix composites are suitable for high-performance structural components in fields such as aerospace, transportation, or military vehicles due to their high strength, good wear resistance, and dimensional stability. SiCw can be easily combined with metals such as Al, Mg, Ni, and Cu using traditional powder metallurgy or squeeze casting methods [147–150].

The research on SiCw-reinforced metal matrix composites began in the mid-1960s when it was recognized that whisker or discontinuous fiber-reinforced composites could rival continuous fiber-reinforced materials in terms of mechanical properties. With the continuous development of SiCw-

reinforced metal matrix composites, numerous scholars and entrepreneurs have conducted in-depth studies on the mechanical properties of SiCw-reinforced different metal matrices.

Table 7 shows the current progress of SiCw-reinforced metal matrix composites. Lianxi and Erde [159] used a twostep squeeze casting method to produce SiCw-reinforced ZK51A magnesium-based composites (SiCw/ZK51A) and investigated the effect of different casting temperatures on the mechanical properties of the composites. Compared to the matrix metal, the composites exhibited significantly improved vield strength, Young's modulus, and tensile strength. The vield strength showed a linear increase with the volume fraction of whiskers in the composite. However, the high strength characteristic of SiCw reinforcement resulted in a reduction in the ductility of the composite. Additionally, when the casting temperature was below 760°C, the yield strength, Young's modulus, and tensile strength increased with temperature. Beyond a critical temperature, the mechanical properties exhibited a decreasing trend, as shown in Figure 15.

Tayebi *et al.* [160] prepared SiCw-reinforced ZK60-based composites using stir casting and studied the high-temperature tensile properties and microstructure of the composites under "as-cast" and "extrusion precipitation hardening" conditions. The study showed that the tensile properties of the composite samples were superior to the unreinforced alloy due to effective load transfer and whisker alignment. Compared to the unreinforced alloy, the composite samples exhibited a 14% increase in yield stress, a 34% increase in ultimate tensile strength, and an 11% increase in Young's modulus. The calculated Young's modulus of the composites agreed well with the predictions of the H-T model. Young's modulus approached its upper limit at temperatures below 250°C and exceeded the upper limit at temperatures above 300°C,

confirming the influence of whisker alignment on the anisotropic properties of the composite. Additionally, microstructural observations revealed micro-pores and voids on the fracture surfaces, indicating that the applied load caused whisker fracture due to the strong whisker/matrix interface (Figure 16).

The H-T model, considering the influence of whisker alignment on the anisotropic properties of the composite, is described by the following equations [161,162]:

$$E_{\rm CL} = \frac{1 + 2\left(\frac{L_{\rm f}}{d}\right)\eta_{\rm L}f}{1 - \eta_{\rm r}f}E_{\rm m},\tag{17}$$

$$E_{\rm CT} = \frac{1 + 2\eta_{\rm T} f}{1 - \eta_{\rm T} f} E_{\rm m},\tag{18}$$

where $E_{\rm CL}$ and $E_{\rm CT}$ are the longitudinal and transverse elastic moduli of the one-dimensional composite, respectively. Furthermore, $L_{\rm f}$ d, and f represent the length, diameter, and volume fraction of the whiskers, respectively. Then, the values of $\eta_{\rm L}$ and $\eta_{\rm T}$ can be calculated using the following equations:

$$\eta_{\rm L} = \frac{E_{\rm rL} - E_{\rm m}}{E_{\rm rL} + 2\left(\frac{L_{\rm f}}{d}\right)E_{\rm m}},\tag{19}$$

$$\eta_{\rm T} = \frac{E_{\rm rT} - E_{\rm m}}{E_{\rm rT} + 2E_{\rm m}},\tag{20}$$

where $E_{\rm rL}$ and $E_{\rm rT}$ are the longitudinal and transverse whisker moduli, respectively.

Yih and Chung [163] used two hot pressing methods to prepare SiCw-reinforced Cu-based composites, as shown in Figure 17, and discussed the variation of the mechanical properties of the composites within SiCw content range from 33 to 54 vol%. When SiCw content was below 49.5%,

Table 7: Summary of SiCw reinforced metal matrix composites

Reinforcement	Matrix	Special process	Whisker loading	Density (g·cm ^{−3})	Properties	Ref.
SiCw	Ti ₆ Al ₄ V	Selective laser melting	1 wt%	_	$\sigma_{\rm u}$ = 1,230.77 ± 30.33; $\sigma_{\rm y}$ = 422.42 ± 4.84; HV = 522.7	[151]
SiCw	ZK60	_	20 wt%	96.34%	$\sigma_{\rm c}$ = 204; $\sigma_{\rm t}$ = 154	[152]
SiCw/SiCp	Ti(C, N)	High-energy ball milling	1.5 wt%SiCp/0.5 wt %SiCw	_	TRS = 2,520.8; K_{IC} = 16.56	[153]
Ti-SiCw	W-20Cu	Hot-press sintering	0.6 wt%	99.1%	TRS = 1,197; TC = 221	[154]
SiCw	Cu, Mg	Stir-casting, warm accumulative	5 wt%	_	$\Delta \sigma_{y} = 41\%; \ \Delta TC = 25\%$	[155]
SiCw	Cu	Co-electrodeposition technology	0.5 g·L ^{−1}	_	TC = 340	[156]
SiCw	ZK60	KOBO extrusion method	10 vol%	_	$\Delta E = 35\%$	[157]
SiCw	Cu	Pulse intermittent deposition, spark plasma sintering	1.1 wt%	_	$\sigma_{\rm y}$ = 346; TC = 261	[158]

 $[\]sigma_{\rm u}$: ultimate tensile strength (MPa); $\sigma_{\rm y}$: Yield strength (MPa); HV: Hardness (GPa); $K_{\rm IC}$: Fracture toughness (MPa·m^{-1/2}); $\sigma_{\rm c}$: Compressive strength (MPa); TC: Thermal conductivity (W·(mK⁻¹)); E: Young's modulus (GPa).

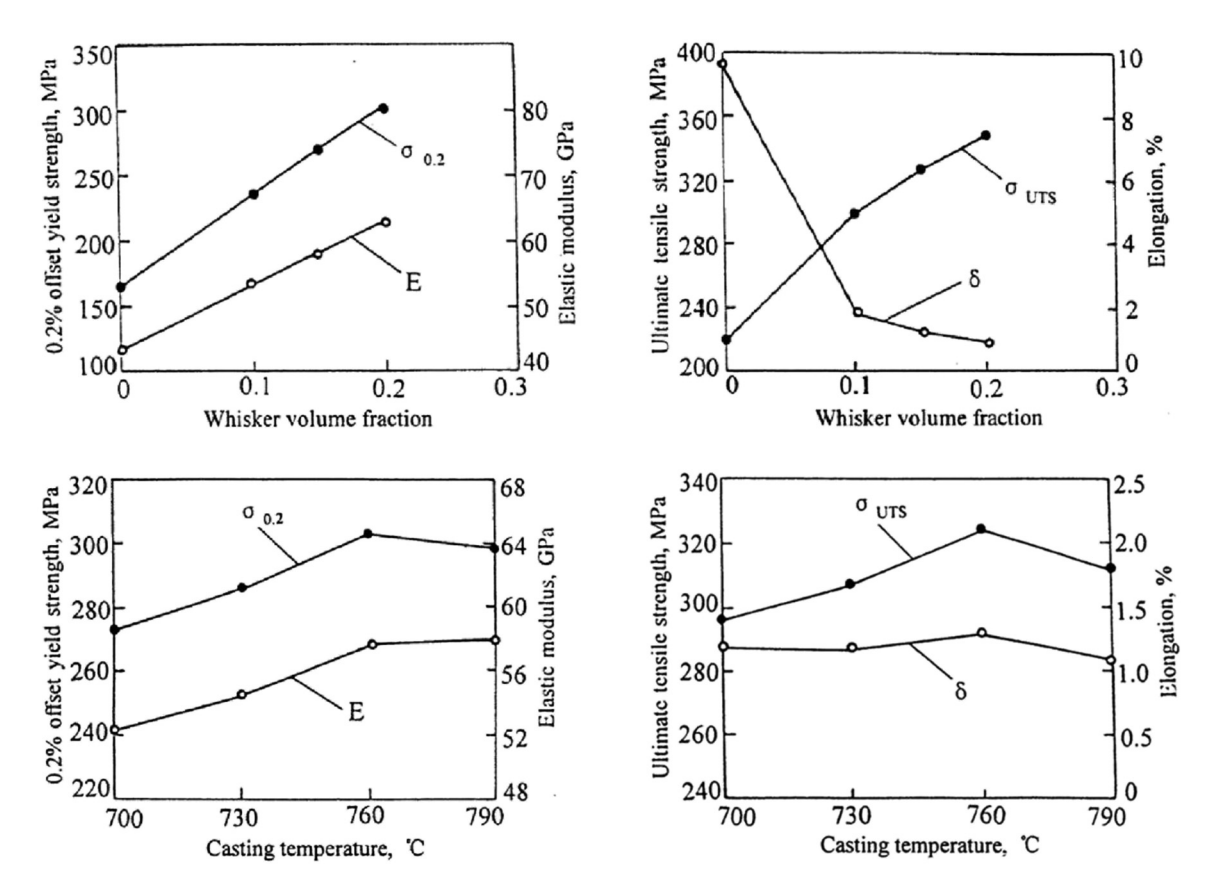


Figure 15: Mechanical properties of SiCw/ZK51A composites [159].

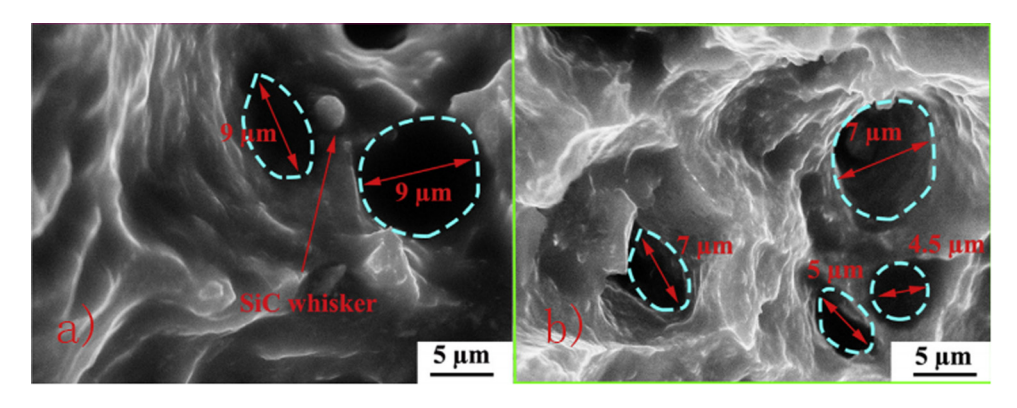
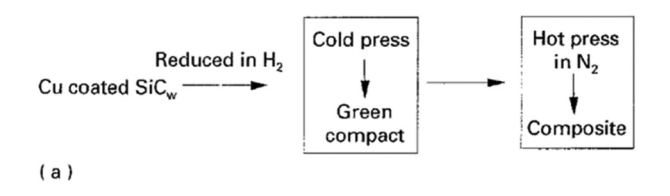


Figure 16: Fracture surfaces of composite samples after tensile testing: (a) at 150°C and (b) at 350°C [160].

the yield strength of the composites prepared by the slurry infiltration method increased with the increase in whisker content, and it decreased slightly when exceeding the critical value due to whisker agglomeration. In contrast, the yield strength of the composites decreased with the increase in SiCw content when using the powder mixing method (Figure 18). This difference was primarily attributed to the variation in porosity of the composites prepared by the two methods, leading to differences in performance.

Li *et al.* [164] prepared SiCw-reinforced copper-based composites using plasma sintering. To enhance the interface bonding between SiCw and the copper matrix, the authors used Ti and SiCp in different proportions to generate ${\rm Ti}_3{\rm SiC}_2$ coating on the surface of SiCw through an *in situ* reaction in a molten state (Table 8). Subsequently, the mixture was plasma-sintered with the copper matrix under reaction conditions of 900°C, 40–50 MPa, and ${\rm H}_2$ atmosphere for 20 min. Experimental results showed that the pre-treated



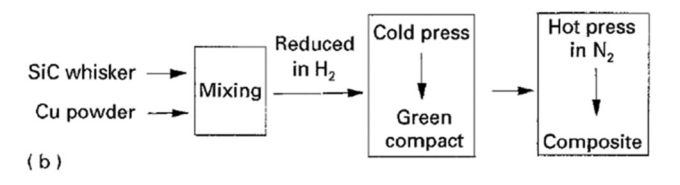


Figure 17: Processing route for Cu-SiCw composites using two hot pressing methods: (a) slurry coating method and (b) powder mixing method [163].

composites exhibited higher tensile strength compared to untreated SiCw. Particularly, the composite prepared under the condition labeled as S2 showed a tensile strength of 525 ± 8.8 MPa, which was an increase of 48 and 47% compared to pure copper metal and untreated SiCw composite, respectively (Figure 19). Interface analysis revealed that the difference in mechanical properties was also attributed to the bonding state between SiCw and the copper matrix.

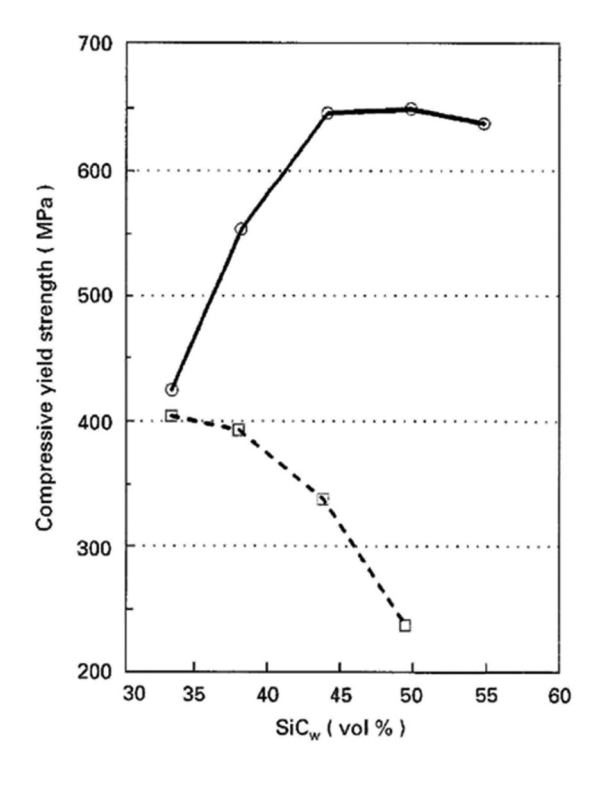
Feng et al. [165] prepared copper-based composites reinforced with SiCw having a consistent Cu coating and

Table 8: Composition of raw materials and reaction condition [164]

Sample	Con	nposition	Reaction		
name	NaCl	KCI	SiC	Ti	condition
SiC@TSC-S1	10	10	2	0.5	1,100°C, 30 min,
SiC@TSC-S2	10	10	2	1	argon protection
SiC@TSC-S3	10	10	2	2	

orientation using powder metallurgy and hot extrusion methods. The composites were fabricated into samples with different whisker orientations, and their electrical conductivity was tested. The influence of SiCw orientation and content on the electrical conductivity of the composites was studied through experiments. The results indicated that SiCw content was the main factor affecting the electrical conductivity of the composites. As the SiCw orientation angle increased, the electrical conductivity of the composites improved (Figure 20). Scanning electron microscopy was used to observe the microstructure of the composites, revealing that SiCw aligned along the hot extrusion direction and were uniformly distributed.

The above studies indicate that the performance of SiCw-reinforced metal matrix composites can be enhanced compared to pure metal materials due to the high strength of SiCw. The strengthening effect of SiCw in SiCw-



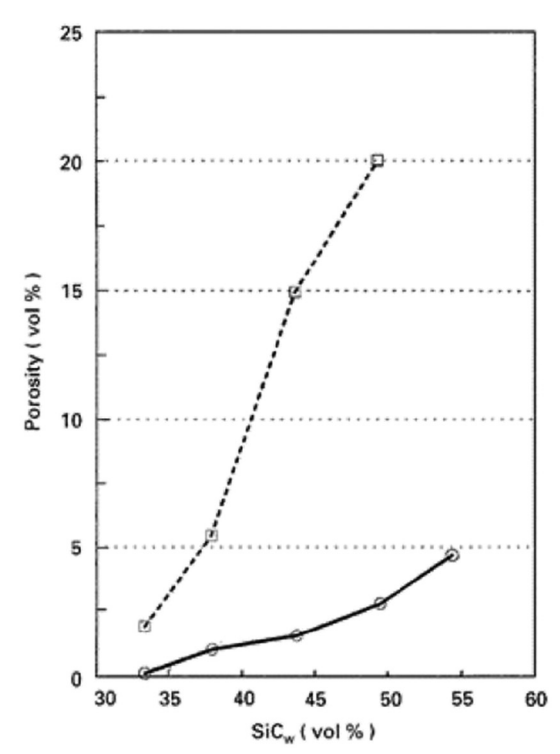


Figure 18: Relationship between compressive yield strength and porosity of Cu–SiCw composites prepared by two methods with SiCw volume fraction: (○) slurry coating method and (□) powder mixing method [163].

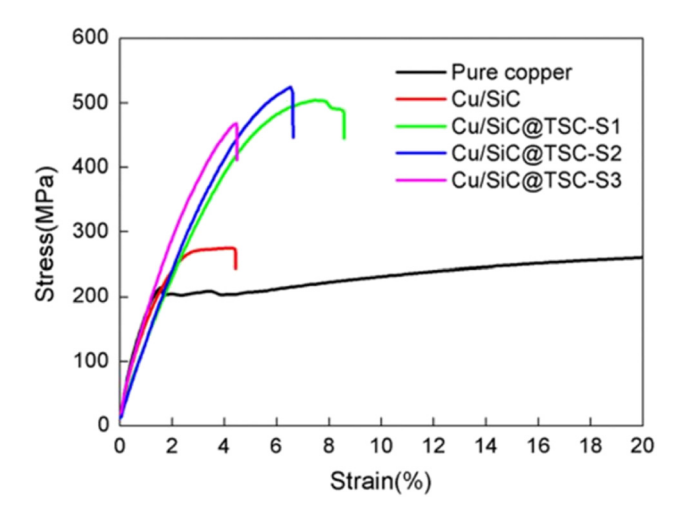


Figure 19: Stress-strain curves of the composites [164].

reinforced metal matrix composites mainly depends on SiCw content and the strength of the interface bonding between SiCw and the metal matrix. When SiCw content is too low, the improvement in composite properties is not significant, and when the content is too high, SiCw agglomeration can degrade the material's performance. Additionally, the importance of interface bonding strength was predicted by previous researchers [166–168]. SiCw and the metal matrix have a significant thermal mismatch, which can lead to high residual stresses and dislocation density at the interface during subsequent heat treatment processes.

3.3 SiCw-reinforced polymer matrix composites

In addition to SiCw-reinforced ceramic and metal matrix composites discussed earlier, polymer matrix composites have attracted attention due to their advantages such as

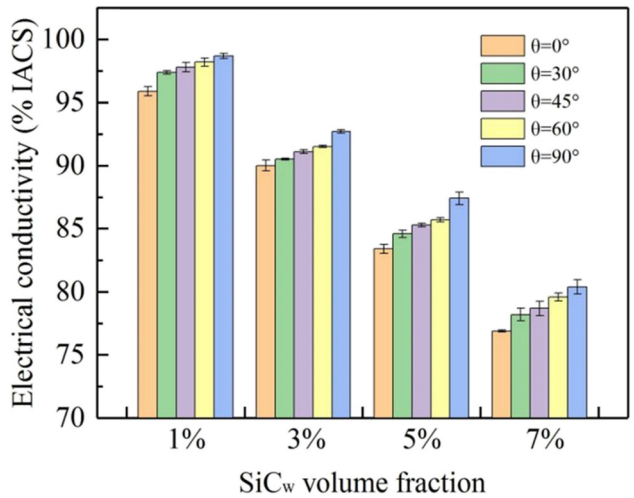


Figure 20: Relationship between electrical conductivity, SiCw spatial distribution, and volume fraction in SiCw/Cu composites [165].

lightweight, good flexibility, and ease of shaping in aerospace, automotive, marine, sports, and leisure equipment industries [169]. Considering the high thermal conductivity and insulating characteristics of SiCw, researchers have started to explore its use in enhancing polymer matrix composites to improve hardness, Young's modulus, thermal conductivity, wear resistance, dielectric constant, *etc.* SiCwreinforced polymer matrix composites have been successfully applied as structural materials or packaging materials in energy storage, micro-electro-mechanical devices, and electromagnetic interference shielding materials [170–174].

Table 9 shows the current progress of SiCw-reinforced polymer matrix composites. Zhou *et al.* [174] prepared SiO₂-encapsulated SiCw through calcination in air and finally obtained SiCw@SiO₂-reinforced polyvinylidene fluoride (PVDF) composites. Fourier transform infrared spectroscopy, X-ray diffraction, and thermogravimetric analysis tests confirmed the formation of an insulating

Table 9: Summary of SiCw reinforced polymer matrix composites

Reinforcement Matrix		Special process	Whisker loading	Properties	Ref.	
SiCw	SR	_	20 wt%	TC = 0.236	[175]	
SiCw/SiO ₂	PVDF	Air-exposure calcination treatment	20 vol%	$\sigma_{\rm t}$ = 30.1	[107]	
BT/β-SiCw	PVDF	_ `	40.0 vol% BT/20.0 vol% β-SiCw	TC = 1.67	[101]	
β-SiCw@SiO ₂	PVDF	Oxidation under air atmosphere	28 wt%	TC = 1.78	[174]	
SiCw@rGO	EP	Stacking bed method	_	TC = 0.51	[176]	
SiCw	EP	Vacuum impregnation	20.63 vol%	TC = 1.79	[177]	
BNNS@ SiCNWs	EP	Ultrasonic technology	20 wt%	TC = 1.17	[178]	
SiCNWs@ Diamond	PDMS	CVD	25 wt%	TC = 0.57	[179]	
β-SiCw@SiO ₂	PVDF	High-temperature oxidation	50 wt%	TC = 2.41	[180]	

TC: Thermal conductivity (W·m⁻¹·K⁻¹); σ_t :Tensile strength (MPa).

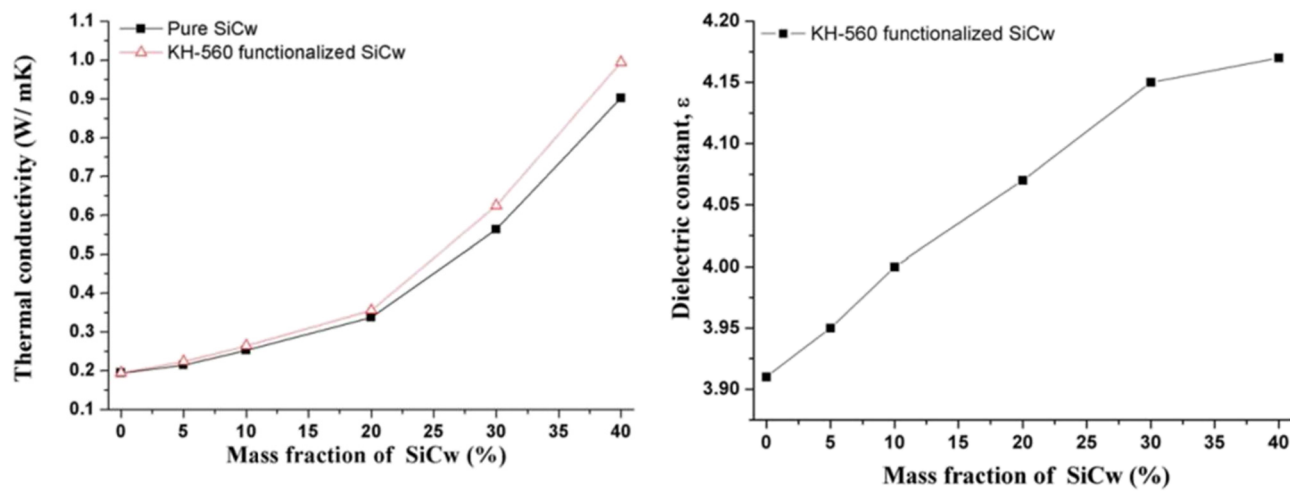


Figure 21: Effects of SiCw mass fraction on the thermal conductivity of b-SiCw/BDM/DBA composites [181].

Figure 22: Effects of SiCw mass fraction on the dielectric constant of b-SiCw/BDM/DBA composites [181].

SiO₂ shell on SiCw surface, and the shell thickness increased with increasing calcination time. Compared to composites with untreated whiskers, SiCw@SiO₂/PVDF composites showed

lower dielectric loss and higher tensile strength and modulus at the same reinforcement content, and the dielectric

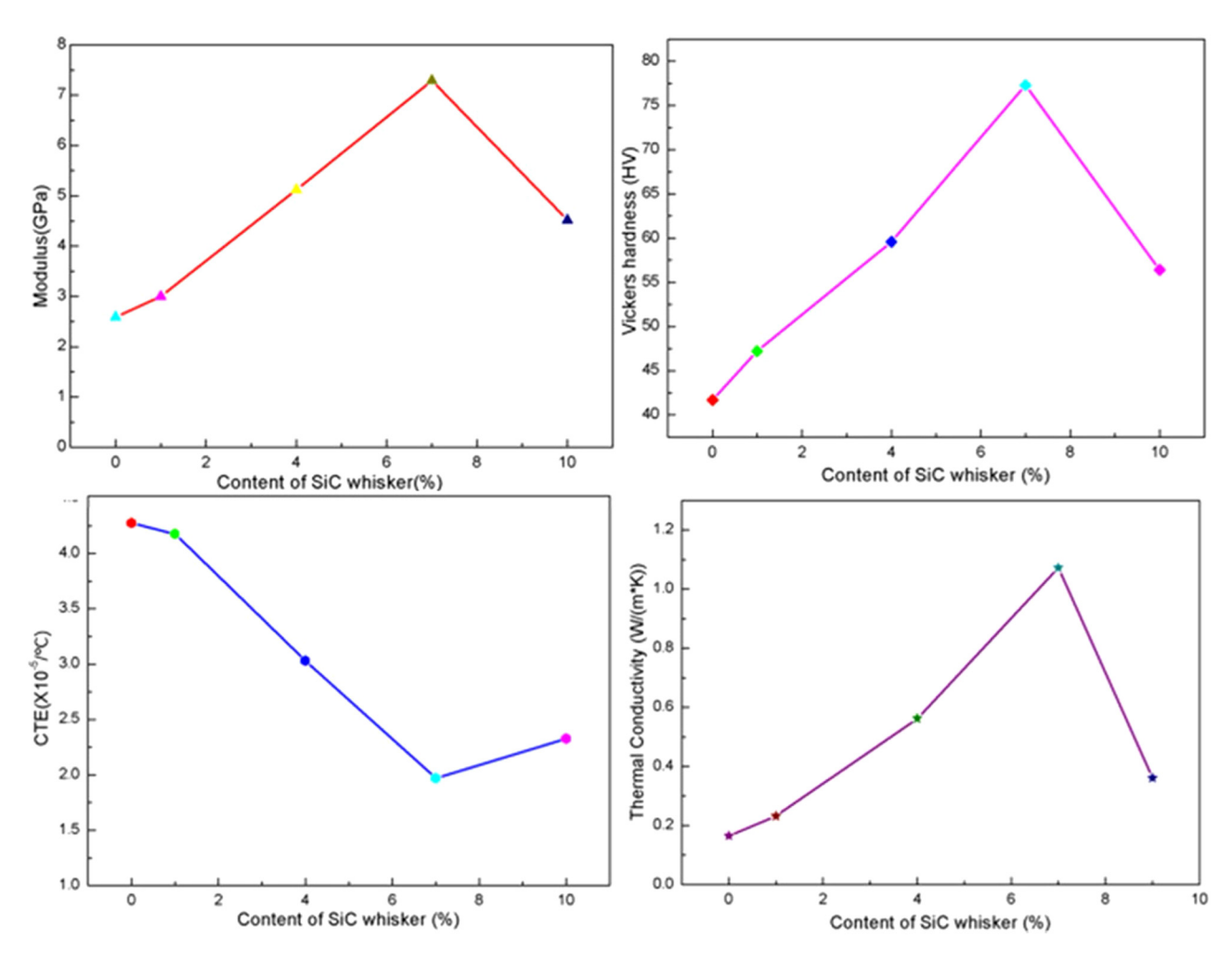


Figure 23: Effects of different SiCw contents on the mechanical properties of the composites [182].

constant and dielectric loss of the composites decreased with increasing calcination time, attributed to the formation of SiO_2 layer enhancing interface compatibility.

Dang *et al.* [181] used powder blending and casting to prepare SiCw-reinforced BDM/DBA composites. The study showed that the composites' mechanical properties were optimal when SiCw content was 10 wt%, and parameters such as dielectric constant and thermal conductivity increased with increasing SiCw content (Figures 21 and 22). When SiCw content was the same, surface treatment of SiCw with KH-560 positively affected the thermal conductivity and mechanical properties of SiCw/BDM/DBA composites.

Liu *et al.* [182] studied the preparation method of SiCwreinforced polyimide (PI) polymer composites and their application in the field of interposers. The study discussed the effect of different doping levels of SiCw in PI on the mechanical and thermal properties of the composites. The results showed that as the mass fraction of SiCw in the PI polymer increased from 0 to 7%, the thermal conductivity of the composites increased from 0.165 to 1.072 W·(m·K⁻¹), Young's modulus increased from 2.58 to 7.29 GPa, and Vickers hardness increased from 41.7 HV to 77.3 HV. However, when the mass fraction exceeded 7%, both the mechanical and thermal properties declined (Figure 23). This is because when the optimal composition is exceeded, SiCw tends to agglomerate in PI polymer, leading to a decrease in the performance of the composites.

Yang *et al.* [183] also reported a composite of SiCw-reinforced SU-8 photoresist to improve the mechanical properties of the polymer. The study discussed the effect of different SiCw content on mechanical performance. The

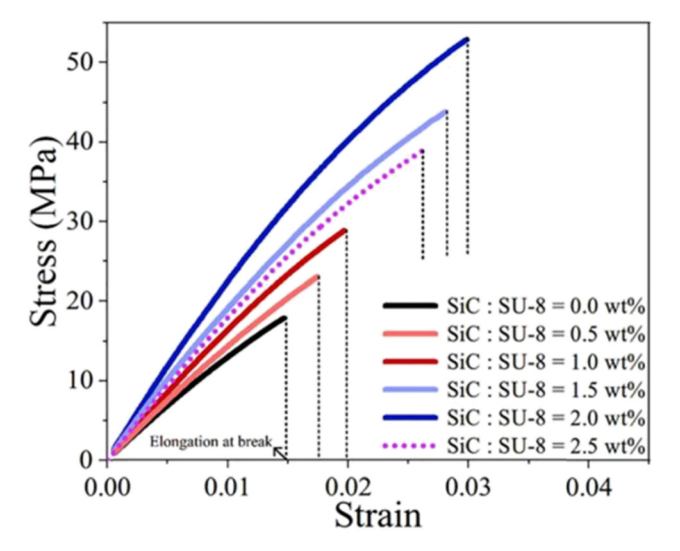


Figure 24: Effects of different SiCw contents on stress–strain behavior of the samples [183].

experimental results showed that when SiCw was uniformly dispersed in the SU-8 photoresist matrix, the composites retained the photo-patterning ability and electrical insulation properties of SU-8. Moreover, when SiCw content was 2 wt%, the elastic modulus and fracture strain of the SU-8 sample increased by 73.88 and 103.4%, respectively (Figure 24).

Zhang *et al.* [184] used SiCw to enhance polystyrene to improve the tensile strength and impact strength of the composites. They found that the optimal SiCw content was 5 wt%, resulting in a tensile strength of 110 MPa and an impact strength of 5.00 kJ·m⁻² for the composites.

Regarding the issue of SiCw aggregation leading to a decline in the mechanical properties of the composites, relevant literature has conducted in-depth research on this matter. For example, the use of surface-active agents to modify and pre-treat SiCw can significantly improve its dispersion, thereby increasing SiCw content in the polymer matrix and ultimately enhancing various aspects of the composites' performance. Xu et al. [173] used chemical modification methods with different silane coupling agents to modify SiCw and then prepared composites with PVDF using a solution casting method. They tested and analyzed the dielectric properties of the materials. The results showed that with an effective SiCw modification method, the composites' dielectric constant could be significantly increased (almost eight times higher) compared to pure PVDF material. Pan [185] also used a KH550 silane coupling agent to modify SiC to improve the composites' resistance to erosion and wear. They systematically discussed the effect of KH550 dosage on the performance and found that the lowest wear rate was achieved with a 1 wt% KH550 dosage. Hui et al. [186] used sodium hexametaphosphate (SHP) and carboxymethyl cellulose (CMC) as dispersants to explore their effects and dispersion mechanisms. The results showed that CMC had a better dispersion effect compared to SHP, and their dispersion mechanisms were distinct. CMC increased SiCw surface hydrophilicity, thereby enhancing the absolute value of SiCw surface potential, while SHP mainly increased the electrostatic repulsion between SiCw particles.

4 Conclusion and recommendation

In summary, SiCw-reinforced composites have shown significant improvements in various aspects of performance. For composites, the correlation between the properties of the matrix and the reinforcement, as well as the order and regularity of interface bonding and distribution, is crucial for enhancing the performance of SiCw-reinforced

composites. The morphology of the matrix material and reinforcement material has a certain impact on their performance, so the preparation process of high-performance reinforcement and matrix is also a means to improve the performance of composite materials. The reinforcing effect of SiCw plays a decisive role in the final performance of SiCw-reinforced composites, and the interface is a key factor influencing the reinforcing effect. Current research primarily focuses on improving the interface compatibility between the matrix and SiCw through interface regulation.

However, there are still some issues in SiCw-reinforced composites. (1) Further research is needed on the structure. functionalization, interface regulation, and the influence of matrix structure on the performance of SiCw-reinforced composites, and to identify their inherent correlations. The influence of the distribution and orientation of reinforcing materials on composite materials has been proven, but there are still significant limitations on the preparation process of micro-nano-level whisker orientation, which requires further improvement. (2) The quantitative relationship between the interface state and the performance of SiCw-reinforced composites remains unclear and requires further in-depth investigation by researchers. (3) The reinforcement mechanism of SiCw in SiCw-reinforced composites is not fully understood. It is essential to establish a relatively unified and more accurate reinforcement mechanism model to explain the influence of SiCw properties and states on the performance of composites. (4) The industrial progress of SiCw-reinforced composites is not satisfactory due to cost and process limitations.

Based on the current research status and development trends of SiCw-reinforced composites, future research in composites can focus on the following three aspects: (1) Interdisciplinary integration is becoming increasingly important. Utilizing mathematical and computer-related software for dynamic simulations of SiCw-reinforced composites and constructing and optimizing mathematical models should be fully explored. (2) Advanced testing techniques can be employed to conduct in-depth studies on the functionalization of SiCw, observe the effects of interface regulation at the microscopic scale, and analyze the underlying mechanisms. (3) Further optimization of the preparation process of SiCw-reinforced composites is needed. In-depth investigations into the effects of various parameters during the preparation process on the structure, morphology, and performance of the composites should be conducted to establish correlations, enabling the production of composites with controllable properties through rational adjustment of preparation process parameters.

Acknowledgments: The authors would like to thank support from the Natural Science Foundation of China (No. 62104151) and the Shanghai Youth Teacher Training Fund (ZZ202212052).

Funding information: The Natural Science Foundation of China (No. 62104151) and the Shanghai Youth Teacher Training Fund (ZZ202212052).

Author contributions: All authors have accepted responsibility for the entire content of this manuscript and approved its submission.

Conflict of interest: The authors state no conflict of interest.

Data availability statement: The data that support the findings of this study are available from the corresponding author upon reasonable request.

References

- [1] Sim, G. D., J. A. Krogstad, K. M. Reddy, K. Y. Xie, G. M. Valentino, T. P. Weihs, et al. Nanotwinned metal MEMS films with unprecedented strength and stability. *Science Advances*, Vol. 3, No. 6, 2017 Jun, id. e1700685.
- [2] Arzt, E. J. Size effects in materials due to microstructural and dimensional constraints: a comparative review. *Acta Materialia*, Vol. 46, No. 16, 1998 Oct, pp. 5611–5626.
- [3] Bogue, R. Non-silicon MEMS-the hard and soft alternatives. Sensor Review, Vol. 36, No. 3, 2016 Jun, pp. 225–230.
- [4] Dai, X. H., Y. Huang, G. F. Ding, and X. Zhao. Optical communication components based on non-silicon MEMS technology. *International Symposium on Photoelectronic Detection and Imaging 2011: Sensor and Micromachined Optical Device Technologies*, Vol. 8191, SPIE, 2011 Sep, pp. 55–61.
- [5] Yang, Z., J. Shi, J. Yao, X. Zhang, G. Ding, and X. Zhao. A laterally driven MEMS inertial switch with double-layer suspended springs for improving single-axis sensitivity. *IEEE Transactions on Components, Packaging and Manufacturing Technology*, Vol. 8, No. 10, 2018 Aug, pp. 1845–1854.
- [6] Olivas, J. D. and S. Bolin. Advancements in MEMS materials and processing technology. *Jom*, Vol. 50, 1998 Jan, pp. 38–43.
- [7] Spearing, S. M. Materials issues in microelectromechanical systems (MEMS). Acta materialia, Vol. 48, No. 1, 2000 Jan, pp. 179–196.
- [8] Varadan, V. K. Nanotechnology: MEMS and NEMS and their applications to smart systems and devices. Smart materials, structures, and systems, Vol. 5062, SPIE, 2003 Oct, pp. 20–43.
- [9] Borkar, T. and S. P. Harimkar. Effect of electrodeposition conditions and reinforcement content on microstructure and tribological properties of nickel composite coatings. *Surface and coatings Technology*, Vol. 205, No. 17–18, 2011 May, pp. 4124–4134.

- [10] Gül, H., F. Kılıç, M. Uysal, S. Aslan, A. Alp, and H. Akbulut. Effect of particle concentration on the structure and tribological properties of submicron particle SiC reinforced Ni metal matrix composite (MMC) coatings produced by electrodeposition. Applied Surface Science, Vol. 258, No. 10, 2012 Mar, pp. 4260-4267.
- Chen, D., H. Yang, R. Luo, L. Wang, J. Huang, and B. Xu. SiC/SiC mini-composites with multilayer ZrSiO4 interphase: Room-temperature properties and toughening mechanism. Ceramics International, Vol. 48, No. 11, 2022 Jun, pp. 15268-15273.
- [12] Mirsaeed-Ghazi, S. M., S. R. Allahkaram, and A. Molaei. Development and investigation of Cu/SiC nano-composite coatings via various parameters of DC electrodeposition. Tribology International, Vol. 134, 2019 Jun, pp. 221-231.
- [13] Chen, S., M. K. Hassanzadeh-Aghdam, and R. Ansari, An analytical model for elastic modulus calculation of SiC whisker-reinforced hybrid metal matrix nanocomposite containing SiC nanoparticles. Journal of Alloys and Compounds, Vol. 767, 2018 Oct, pp. 632–641.
- Zhang, Z., Y. Liu, and H. Liu. Mechanical properties and microstructure of spark plasma sintered Al2O3-SiCw-Si3N4 composite ceramic tool materials. Ceramics International, Vol. 48, No. 4, 2022 Feb. pp. 5527-5534.
- [15] Kahar, S. M., C. H. Voon, C. C. Lee, U. Hashim, M. K. Md Arshad, B. Y. Lim, et al. Synthesis of SiC nanowhiskers from graphite and silica by microwave heating. Materials Science-Poland, Vol. 34, No. 4, 2016 Dec, pp. 770-779.
- Iveković, A., S. Novak, G. Dražić, D. Blagoeva, and S. G. de Vicente. [16] Current status and prospects of SiCf/SiC for fusion structural applications. Journal of the European Ceramic Society, Vol. 33, No. 10, 2013 Sep, pp. 1577-1589.
- Liu, L., M. Kang, and X. Wang. Research on Surface Chemistry and [17] Mechanical Properties of SiC Whiskers. Ordnance Material Science and Engineering, Vol. 5, 2000, pp. 59-64.
- Katoh, Y., K. Ozawa, C. Shih, T. Nozawa, R. J. Shinavski, A. Hasegawa, et al. Continuous SiC fiber, CVI SiC matrix composites for nuclear applications: Properties and irradiation effects. Journal of Nuclear Materials, Vol. 448, No. 1-3, 2014 May, pp. 448-476.
- Shen, D., M. Wang, Y. Wu, Z. Liu, Y. Cao, T. Wang, et al. Enhanced thermal conductivity of epoxy composites with core-shell SiC@ SiO₂ nanowires. *High Voltage*, Vol. 2, No. 3, 2017 Sep, pp. 154–160.
- Lu, D., L. Zhang, S. Cheng, D. Shi, K. Zhang, W. Shao, et al. Microstructure control of SiCw/SiC composites based on SLS technology. Journal of the European Ceramic Society, Vol. 42, No. 9, 2022 Aug, pp. 3747-3758.
- Lu, D., S. Cheng, L. Zhang, D. Shi, M. Fan, and T. Zeng. Study on growth factors of SiC whisker in situ in SiCW/SiC composites based on selective laser sintering technology. Ceramics International, Vol. 49, No. 7, 2023 Apr, pp. 10673-10681.
- [22] Hao, S. M., J. P. Xie, A. Q. Wang, W. Y. Wang, and J. W. Li. Strengthening mechanism of micrometer SiC particle reinforced aluminum matrix composites. Transactions of Materials and Heat Treatment, Vol. 37, 2016, pp. 1-6.
- Zhou, Y. Investigation on process optimization and organization ana-[23] lysis of SiC particles reinforced aluminum matrix composites by selective laser melting. Master's thesis, Beijing University of Technology.
- [24] Hua, B. and H. Zhu. State of the art of particle reinforced aluminum matrix composites. Journal of Materials Science & Engineering, Vol. 33, No. 1, 2015, pp. 151-156.
- [25] Kashyap, B. P. and K. Tangri. On the Hall-Petch relationship and substructural evolution in type 316L stainless steel. Acta Metallurgica et Materialia, Vol. 43, No. 11, 1995 Nov, pp. 3971-3981.

- [26] Hall, E. O. The deformation and ageing of Mid Steel: III discussion of results. Proceedings of the Physical Society Section B, Vol. 64, 1951, id. 53.
- [27] Zhu, Y. Z., S. Z. Wang, B. L. Li, Z. M. Yin, Q. Wan, and P. Liu. Grain growth and microstructure evolution based mechanical property predicted by a modified Hall-Petch equation in hot worked Ni76Cr19AlTiCo alloy. Materials & Design, Vol. 55, 2014 Mar, pp. 456-462.
- [28] Deng, H., X. Wan, K. Ren, X. Li, Y. Shi, Z. Bai, et al. Reviews on fabrication, interface modification and reinforcing mechanism of nanocarbon/aluminum composites. Journal of Solid Rocket Technology, Vol. 46, No. 2, 2023, pp. 231-252.
- [29] Casati, R. and M. Vedani. Metal matrix composites reinforced by nano-particles-a review. Metals. Vol. 4. No. 1, 2014 Mar. pp. 65–83.
- [30] Park, J. G., D. H. Keum, and Y. H. Lee. Strengthening mechanisms in carbon nanotube-reinforced aluminum composites. Carbon, Vol. 95, 2015 Dec, pp. 690-698.
- Tjong, S. C. Recent progress in the development and properties of novel metal matrix nanocomposites reinforced with carbon nanotubes and graphene nanosheets. Materials Science and Engineering: R: Reports, Vol. 74, No. 10, 2013 Oct, pp. 281-350.
- [32] Wang, M., D. Chen, Z. Chen, Y. Wu, F. Wang, N. Ma, et al. Mechanical properties of in situ TiB2/A356 composites. Materials Science and Engineering: A, Vol. 590, 2014 Jan, pp. 246-254.
- [33] Zhang, Z. and D. L. Chen. Consideration of Orowan strengthening effect in particulate-reinforced metal matrix nanocomposites: A model for predicting their yield strength. Scripta Materialia, Vol. 54, No. 7, 2006 Apr, pp. 1321-1326.
- [34] Arsenault, R. J. and N. Shi. Dislocation generation due to differences between the coefficients of thermal expansion. Materials Science and Engineering, Vol. 81, 1986 Aug, pp. 175-187.
- Gao, X. L. and K. Li. A shear-lag model for carbon nanotubereinforced polymer composites. International Journal of Solids and Structures, Vol. 42, No. 5-6, 2005 Mar, pp. 1649-1667.
- [36] Ryu, H. J., S. I. Cha, and S. H. Hong. Generalized shear-lag model for load transfer in SiC/Al metal-matrix composites. Journal of Materials Research, Vol. 18, No. 12, 2003 Dec, pp. 2851–2858.
- Kelly, A. and A. W. Tyson. Tensile properties of fibre-reinforced [37] metals: copper/tungsten and copper/molybdenum. Journal of the Mechanics and Physics of Solids, Vol. 13, No. 6, 1965 Dec, pp. 329-350.
- Li, J., X. Zhang, and L. Geng. Effect of heat treatment on interfacial [38] bonding and strengthening efficiency of graphene in GNP/Al composites. Composites Part A: Applied Science and Manufacturing, Vol. 121, 2019 Jun, pp. 487-498.
- [39] Chen, B., S. Li, H. Imai, L. Jia, J. Umeda, M. Takahashi, et al. Load transfer strengthening in carbon nanotubes reinforced metal matrix composites via in situ tensile tests. Composites Science and Technology, Vol. 113, 2015 Jun, pp. 1-8.
- [40] Zhou, W., G. Yamamoto, Y. Fan, H. Kwon, T. Hashida, and A. Kawasaki. In situ characterization of interfacial shear strength in multi-walled carbon nanotube reinforced aluminum matrix composites. Carbon, Vol. 106, 2016 Sep, pp. 37-47.
- [41] Shao, P., G. Chen, B. Ju, W. Yang, Q. Zhang, Z. Wang, et al. Effect of hot extrusion temperature on graphene nanoplatelets reinforced Al6061 composite fabricated by pressure infiltration method. Carbon, Vol. 162, 2020 Jun, pp. 455-464.
- [42] Long, F., X. Guo, K. Song, S. Jia, V. Yakubov, S. Li, et al. Synergistic strengthening effect of carbon nanotubes (CNTs) and titanium diboride (TiB2) microparticles on mechanical properties of copper

- matrix composites. *Journal of Materials Research and Technology*, Vol. 9, No. 4, 2020 Jul, pp. 7989–8000.
- [43] Jin, Z. L., S. L. Li, and W. Li. Performance and application of the complex material reinforced by whiskers. *Journal of Salt Lake Research*, Vol. 4, 2003, pp. 10–21.
- [44] Qingfeng, Z., D. Limin, W. Chen, W. Chang-an, and H. Yong. Improvement of mechanical properties of Al2O3/Ti3SiC2 multilayer ceramics by adding SiC whiskers into Al2O3 layers. *Ceramics international*, Vol. 33, No. 3, 2007 Apr, pp. 385–388.
- [45] Fukasawa, T., Y. Goto, and M. Kato. Fracture behaviour of SiC whisker/Si3N4 multi-layered composites. *Journal of Materials Science Letters*, Vol. 16, No. 17, 1997 Sep, pp. 1423–1425.
- [46] LLorca, J. Fatigue of particle-and whisker-reinforced metal-matrix composites. *Progress in Materials Science*, Vol. 47, No. 3, 2002 Jan, pp. 283–353.
- [47] Chen, E. F. and D. Chen. The development of whisker-reinforced polymer composites mechanisms. *Gaofenzi Cailiao Kexue yu Gongcheng(Polymer Materials Science & Engineering)*, Vol. 22, No. 2, 2006 Mar, pp. 20–24.
- [48] Guo, R., Z. Li, L. Li, R. Zheng, and C. Ma. Toughening mechanism and oxidation resistance of SiC whisker-toughened SiAlCN ceramics. *Ceramics International*, Vol. 50, No. 6, 2024 Mar, pp. 8853–8864.
- [49] Homeny, J. and W. L. Vaughn. Whisker-reinforced ceramic matrix composites. MRS Bulletin, Vol. 12, No. 7, 1987 Nov, pp. 66–72.
- [50] Rahman, A. S. Nanofiber reinforcement of a geopolymer matrix for improved composite materials mechanical performance. *Doctoral dissertation*, Colorado State University.
- [51] Wei, W. E., L. I. Wei, L. I. Qi, and C. A. Lamei. Effect of SiC whisker on properties of SiBCN based ceramic composites. *Journal of Materials Engineering*, Vol. 51, No. 5, 2023 May, pp. 138–145.
- [52] Shirvanimoghaddam, K., S. U. Hamim, M. K. Akbari, S. M. Fakhrhoseini, H. Khayyam, A. H. Pakseresht, et al. Carbon fiber reinforced metal matrix composites: Fabrication processes and properties. *Composites Part A: Applied Science and Manufacturing*, Vol. 92, 2017 Jan, pp. 70–96.
- [53] Zhang, L. Preparation of silicon carbide ceramics reinforced by particles or/and whiskers and their application in mechanical seals. *Doctoral dissertation*, Zhejjang University, Hangzhou.
- [54] Dong, R., W. Yang, P. Wu, M. Hussain, G. Wu, and L. Jiang. High content SiC nanowires reinforced Al composite with high strength and plasticity. *Materials Science and Engineering: A*, Vol. 630, 2015 Apr, pp. 8–12.
- [55] Lin, H., X. Guo, K. Song, S. Li, J. Feng, X. Zhang, et al. Synergistic strengthening effect of tungsten carbide (WC) particles and silicon carbide whiskers (SiCw) on mechanical properties of Cu–Al2O3 composite. *Journal of Materials Research and Technology*, Vol. 15, 2021 Nov, pp. 2837–2847.
- [56] Ungár, T., A. Borbély, G. R. Goren-Muginstein, S. Berger, and A. R. Rosen. Particle-size, size distribution and dislocations in nanocrystalline tungsten-carbide. *Nanostructured Materials*, Vol. 11, No. 1, 1999 Feb, pp. 103–113.
- [57] Ahn, J. J. and S. Ochiai. The effect of wear environment temperature on the wear behavior and friction coefficient of SiCw/Al composite. *Journal of composite materials*, Vol. 37, No. 12, 2003 Jun, pp. 1083–1092.
- [58] Akhtar, W., J. Sun, P. Sun, W. Chen, and Z. Saleem. Tool wear mechanisms in the machining of Nickel based super-alloys: A review. *Frontiers of Mechanical Engineering*, Vol. 9, 2014 Jun, pp. 106–119.

- [59] Bushlya, V., J. Zhou, P. Avdovic, and J. E. Ståhl. Wear mechanisms of silicon carbide-whisker-reinforced alumina (Al 2 O 3-SiC w) cutting tools when high-speed machining aged Alloy 718. The International Journal of Advanced Manufacturing Technology, Vol. 68, 2013 Sep, pp. 1083–1093.
- [60] Jianxin, D. Friction and wear behaviour of Al2O3/TiB2/SiCw ceramic composites at temperatures up to 800 C. Ceramics international, Vol. 27, No. 2, 2001 Jan, pp. 135–141.
- [61] Paul, T. R., M. K. Mondal, and M. Mallik. Abrasive wear performance and wear map of ZrB2-MoSi2-SiCw composites. *Journal of the European Ceramic Society*, Vol. 41, No. 6, 2021 Jun, pp. 3227–3251.
- [62] Smirnov, A., P. Peretyagin, N. W. Solis Pinargote, I. Gershman, and J. F. Bartolome. Wear behavior of graphene-reinforced alumina-silicon carbide whisker nanocomposite. Nanomaterials, Vol. 9, No. 2, 2019 Jan, pp. 151.
- [63] Sun, J., Y. Chen, P. Zhai, Y. Zhou, J. Zhao, and Z. Huang. Tribological performance of binderless tungsten carbide reinforced by multilayer graphene and SiC whisker. *Journal of the European Ceramic Society*, Vol. 42, No. 12, 2022 Sep, pp. 4817–4824.
- [64] Suresha, B., K. Adappa, and N. K. Subramani. Mechanical and tribological behaviours of epoxy hybrid composites reinforced by carbon fibers and silicon carbide whiskers. *Materials Today: Proceedings*, Vol. 5, No. 8, 2018 Jan, pp. 16658–16668.
- [65] Du, J., G. Liu, Y. Song, Z. Deng, and F. Xie. Study on the Tribological Performance of Nano-SiCw Reinforced Cu-based. CompositesJournal of Academy of Armored Force Engineering, Vol. 23, No. 1, 2009, pp. 77–80.
- [66] Ke, Y. Research on microstructure and properties of nano-SiC whisker modified Ti(C,N)-based cermets. *Master's thesis*, Huazhong University of Science & Technology.
- [67] Zhou, W., S. Qi, Q. An, H. Zhao, and N. Liu. Thermal conductivity of boron nitride reinforced polyethylene composites. *Materials Research Bulletin*, Vol. 42, No. 10, 2007 Oct, pp. 1863–1873.
- [68] Kim, K., M. Kim, Y. Hwang, and J. Kim. Chemically modified boron nitride-epoxy terminated dimethylsiloxane composite for improving the thermal conductivity. *Ceramics International*, Vol. 40, No. 1, 2014 Jan, pp. 2047–2056.
- [69] He, J., H. Wang, Z. Su, Y. Guo, X. Tian, Q. Qu, et al. Thermal conductivity and electrical insulation of epoxy composites with graphene-SiC nanowires and BaTiO3. *Composites Part A: Applied Science and Manufacturing*, Vol. 117, 2019 Feb, pp. 287–298.
- [70] Hu, P., S. Dong, X. Zhang, K. Gui, G. Chen, and Z. Hu. Synthesis and characterization of ultralong SiC nanowires with unique optical properties, excellent thermal stability and flexible nanomechanical properties. *Scientific Reports*, Vol. 7, No. 1, 2017 Jun, id. 3011.
- [71] Ma, J., Y. Liu, P. Hao, J. Wang, and Y. Zhang. Effect of different oxide thickness on the bending Young's modulus of SiO₂@ SiC nanowires. Scientific reports, Vol. 6, No. 1, 2016 Jan, id. 18994.
- [72] Tang, D., J. Su, M. Kong, Z. Zhao, Q. Yang, Y. Huang, et al. Preparation and properties of epoxy/BN highly thermal conductive composites reinforced with S i C whisker. *Polymer Composites*, Vol. 37, No. 9, 2016 Sep, pp. 2611–2621.
- [73] Gu, J., Q. Zhang, J. Dang, C. Yin, and S. Chen. Preparation and properties of polystyrene/SiCw/SiCp thermal conductivity composites. *Journal of applied polymer science*, Vol. 124, No. 1, 2012 Apr, pp. 132–137.
- [74] Li, B., M. Yuan, S. Zhang, R. Rajagopalan, and M. T. Lanagan. Abnormal high voltage resistivity of polyvinylidene fluoride and

- implications for applications in high energy density film capacitors. Applied Physics Letters, Vol. 113, No. 19, 2018 Nov, id. 193903.
- [75] Xu, X., J. Zhou, and J. Chen. Thermal transport in conductive polymer-based materials. Advanced Functional Materials, Vol. 30, No. 8, 2020 Feb, id. 1904704.
- Li, S., S. Qi, N. Liu, and P. Cao. Study on thermal conductive BN/ novolac resin composites. Thermochimica Acta, Vol. 523, No. 1-2, 2011 Aug, pp. 111-115.
- [77] Saleem, A., Y. Zhang, H. Gong, M. K. Majeed, M. Z. Ashfaq, J. Jing, et al. Carbon nanostructure-reinforced SiC w/Si 3 N 4 composite with enhanced thermal conductivity and mechanical properties. RSC Advances, Vol. 10, No. 25, 2020, pp. 15023-15029.
- Shen, Z. and J. Feng. Achieving vertically aligned SiC microwires networks in a uniform cold environment for polymer composites with high through-plane thermal conductivity enhancement. Composites Science and Technology, Vol. 170, 2019 Jan, pp. 135–140.
- [79] Pan, C., K. Kou, Y. Zhang, Z. Li, T. Ji, and G. Wu. Investigation of the dielectric and thermal conductive properties of core-shell structured HGM@ hBN/PTFE composites. Materials Science and Engineering: B, Vol. 238, 2018 Dec, pp. 61-70.
- Wang, Z., M. Yang, Y. Cheng, J. Liu, B. Xiao, S. Chen, et al. Dielectric [80] properties and thermal conductivity of epoxy composites using quantum-sized silver decorated core/shell structured alumina/ polydopamine. Composites Part A: Applied Science and Manufacturing, Vol. 118, 2019 Mar, pp. 302-311.
- [81] Cheng, S. C. and R. I. Vachon. The prediction of the thermal conductivity of two and three phase solid heterogeneous mixtures. International Journal of Heat and Mass Transfer, Vol. 12, No. 3, 1969 Mar, pp. 249-264.
- Nielsen, L. E. Generalized equation for the elastic moduli of [82] composite materials. Journal of Applied Physics, Vol. 41, No. 11, 1970 Oct, pp. 4626-4627.
- Ott, H. J. Thermal conductivity of composite materials. Plastics and rubber processing and applications, Vol. 1, No. 1, 1981, pp. 9–24.
- Agari, Y. and T. Uno. Estimation on thermal conductivities of filled polymers. Journal of Applied Polymer Science, Vol. 32, No. 7, 1986 Nov, pp. 5705-5712.
- Hasselman, D. P. and L. F. Johnson. Effective thermal conductivity of composites with interfacial thermal barrier resistance. Journal of Composite Materials, Vol. 21, No. 6, 1987 Jun, pp. 508-515.
- Zhou, W., C. Wang, Q. An, and H. Ou. Thermal properties of heat [86] conductive silicone rubber filled with hybrid fillers. Journal of composite materials, Vol. 42, No. 2, 2008 Jan, pp. 173-187.
- Agari, Y., A. Ueda, and S. Nagai. Thermal conductivity of a polymer composite. Journal of Applied Polymer Science, Vol. 49, No. 9, 1993 Sep, pp. 1625-1634.
- [88] Gu, J. W., Q. Zhang, J. Zhang, and W. Wang. Studies on the preparation of polystyrene thermal conductivity composites. Polymer-Plastics Technology and Engineering, Vol. 49, No. 13, 2010 Sep, pp. 1385-1389.
- Zhou, W., C. Wang, T. Ai, K. Wu, F. Zhao, and H. Gu. A novel fiberreinforced polyethylene composite with added silicon nitride particles for enhanced thermal conductivity. Composites Part A: Applied Science and Manufacturing, Vol. 40, No. 6-7, 2009 Jul,
- Zhou, W., S. Qi, C. Tu, H. Zhao, C. Wang, and J. Kou. Effect of the particle size of Al2O3 on the properties of filled heat-conductive silicone rubber. Journal of Applied Polymer Science, Vol. 104, No. 2, 2007 Apr, pp. 1312-1318.

- [91] Xie, B. H., X. Huang, and G. J. Zhang. High thermal conductive polyvinyl alcohol composites with hexagonal boron nitride microplatelets as fillers. Composites Science and Technology, Vol. 85, 2013 Aug, pp. 98-103.
- [92] Fan, B., M. Zhou, C. Zhang, D. He, and J. Bai. Polymer-based materials for achieving high energy density film capacitors. Progress in Polymer Science, Vol. 97, 2019 Oct, id. 101143.
- Jung, H. M., J. H. Kang, S. Y. Yang, J. C. Won, and Y. S. Kim. Barium [93] titanate nanoparticles with diblock copolymer shielding layers for high-energy density nanocomposites. Chemistry of Materials, Vol. 22, No. 2, 2010 Jan, pp. 450-456.
- [94] Valeev, E. F., V. Coropceanu, D. A. da Silva Filho, S. Salman, and J. L. Brédas. Effect of electronic polarization on charge-transport parameters in molecular organic semiconductors. Journal of the American Chemical Society, Vol. 128, No. 30, 2006 Aug, pp. 9882-9886.
- Nan, C. W., Y. Shen, and J. Ma. Physical properties of composites near percolation. Annual Review of Materials Research, Vol. 40, No. 1, 2010 Aug, pp. 131-151.
- [96] Zhang, L. I. and Z. Y. Cheng. Development of polymer-based 0-3 composites with high dielectric constant. Journal of Advanced Dielectrics, Vol. 1, No. 4, 2011 Oct, pp. 389-406.
- Dang, Z. M., J. K. Yuan, S. H. Yao, and R. J. Liao. Flexible nanodi-[97] electric materials with high permittivity for power energy storage. Advanced Materials, Vol. 25, No. 44, 2013 Nov, pp. 6334-6365.
- Qi, L., B. I. Lee, S. Chen, W. D. Samuels, and G. J. Exarhos. High-[98] dielectric-constant silver-epoxy composites as embedded dielectrics. Advanced Materials, Vol. 17, No. 14, 2005 Jul, pp. 1777-1781, (PNNL-SA-44805).
- Zhang, Z., Y. Gu, S. Wang, M. Li, J. Bi, and Z. Zhang. Enhancement [99] of dielectric and electrical properties in BT/SiC/PVDF three-phase composite through microstructure tailoring. Composites Part A: Applied Science and Manufacturing, Vol. 74, 2015 Jul, pp. 88–95.
- Cao, J. P., J. Zhao, X. Zhao, G. H. Hu, and Z. M. Dang. Preparation and characterization of surface modified silicon carbide/polystyrene nanocomposites. Journal of Applied Polymer Science, Vol. 130, No. 1, 2013 Oct, pp. 638-644.
- Li, Y., X. Huang, Z. Hu, P. Jiang, S. Li, and T. Tanaka. Large dielectric constant and high thermal conductivity in poly (vinylidene fluoride)/barium titanate/silicon carbide three-phase nanocomposites. ACS Applied Materials & Interfaces, Vol. 3, No. 11, 2011 Nov, pp. 4396-4403.
- [102] Zhong, S. L., Z. M. Dang, W. Y. Zhou, and H. W. Cai. Past and future on nanodielectrics. IET Nanodielectrics, Vol. 1, No. 1, 2018 Apr,
- [103] Rasel, R. K., C. Gunes, Q. M. Marashdeh, and F. L. Teixeira. Exploiting the Maxwell-Wagner-Sillars effect for displacementcurrent phase tomography of two-phase flows. IEEE Sensors Journal, Vol. 17, No. 22, 2017 Sep, pp. 7317-7324.
- [104] Zhang, Y., Y. Wang, Y. Deng, M. Li, and J. Bai. Enhanced dielectric properties of ferroelectric polymer composites induced by metalsemiconductor Zn-ZnO core-shell structure. ACS Applied Materials & Interfaces, Vol. 4, No. 1, 2012 Jan, pp. 65-68.
- Zhou, W., Q. Chen, X. Sui, L. Dong, and Z. Wang. Enhanced [105] thermal conductivity and dielectric properties of Al/β-SiCw/PVDF composites. Composites Part A: Applied Science and Manufacturing, Vol. 71, 2015 Apr, pp. 184-191.
- [106] Zhou, W., L. Xu, L. Jiang, J. Peng, Y. Gong, X. Liu, et al. Towards suppressing loss tangent: Effect of SiO₂ coating layer on dielectric

- properties of core-shell structure flaky Cu reinforced PVDF composites. *Journal of Alloys and Compounds*, Vol. 710, 2017 Jul, pp. 47–56.
- [107] Bi, J., Y. Gu, Z. Zhang, S. Wang, M. Li, and Z. Zhang. Core–shell SiC/ SiO₂ whisker reinforced polymer composite with high dielectric permittivity and low dielectric loss. *Materials & Design*, Vol. 89, 2016 Jan, pp. 933–940.
- [108] Li, B. and E. Manias. Increased dielectric breakdown strength of polyolefin nanocomposites via nanofiller alignment. Mrs Advances, Vol. 2, 2017 Jan, pp. 357–362.
- [109] Zhou, W., Y. Kou, M. Yuan, B. Li, H. Cai, Z. Li, et al. Polymer composites filled with core@ double-shell structured fillers: Effects of multiple shells on dielectric and thermal properties. Composites Science and Technology, Vol. 181, 2019 Sep, id. 107686.
- [110] Zhou, W., F. Zhang, M. Yuan, B. Li, J. Peng, Y. Lv, et al. Improved dielectric properties and thermal conductivity of PVDF composites filled with core-shell structured Cu@ CuO particles. *Journal of Materials Science: Materials in Electronics*, Vol. 30, 2019 Oct, pp. 18350–18361.
- [111] Zhou, W., Y. Gong, L. Tu, L. Xu, W. Zhao, J. Cai, et al. Dielectric properties and thermal conductivity of core-shell structured Ni@ NiO/poly (vinylidene fluoride) composites. *Journal of Alloys and Compounds*, Vol. 693, 2017 Feb, pp. 1–8.
- [112] Luo, H., X. Zhou, C. Ellingford, Y. Zhang, S. Chen, K. Zhou, et al. Interface design for high energy density polymer nanocomposites. *Chemical Society Reviews*, Vol. 48, No. 16, 2019, pp. 4424–4465.
- [113] Petrovic, J. J. and R. C. Hoover. Tensile fracture behaviour of long SiC whiskers. *Journal of materials science*, Vol. 22, 1987 Feb, pp. 517–522.
- [114] Petrovic, J. J. and R. B. Roof. Fracture toughness of a beta-SiC whisker. *Journal of the American Ceramic Society*, Vol. 67, No. 10, 1984 Oct, id. C-219.
- [115] Sun, Q. and W. Li. Inorganic-whisker-reinforced polymer composites: synthesis, properties and applications, CRC Press, Florida, USA, 2015 Aug.
- [116] Liu, Y., L. Cheng, L. Zhang, Y. Hua, and W. Yang. Microstructure and properties of particle reinforced silicon carbide and silicon nitride ceramic matrix composites prepared by chemical vapor infiltration. *Materials Science and Engineering: A*, Vol. 475, No. 1–2, 2008 Feb, pp. 217–223.
- [117] Magnani, G., G. Beltrami, G. L. Minoccari, and L. Pilotti. Pressureless sintering and properties of αSiC–B4C composite. *Journal of the European Ceramic Society*, Vol. 21, No. 5, 2001 May, pp. 633–638.
- [118] Li, S., Y. Zhang, J. Han, and Y. Zhou. Fabrication and characterization of SiC whisker reinforced reaction bonded SiC composite. *Ceramics International*, Vol. 39, No. 1, 2013 Jan, pp. 449–455.
- [119] Xie, Y., L. Cheng, L. Li, H. Mei, and L. Zhang. Fabrication of laminated SiCw/SiC ceramic composites by CVI. *Journal of the European Ceramic Society*, Vol. 33, No. 10, 2013 Sep, pp. 1701–1706.
- [120] Hua, Y., L. Zhang, L. Cheng, Z. Li, and J. Du. Microstructure and high temperature strength of SiCW/SiC composites by chemical vapor infiltration. *Materials Science and Engineering: A*, Vol. 527, No. 21–22, 2010 Aug, pp. 5592–5595.
- [121] Zhu, S., M. Mizuno, Y. Kagawa, J. Cao, Y. Nagano, and H. Kaya. Creep and fatigue behavior in Hi-Nicalon-fiber-reinforced silicon carbide composites at high temperatures. *Journal of the American Ceramic Society*, Vol. 82, No. 1, 1999 Jan, pp. 117–128.

- [122] Chen, L., X. Yin, X. Fan, M. Chen, X. Ma, L. Cheng, et al. Mechanical and electromagnetic shielding properties of carbon fiber reinforced silicon carbide matrix composites. *Carbon*, Vol. 95, 2015 Dec, pp. 10–19.
- [123] Xu, Y., Y. Zhang, L. Cheng, L. Zhang, J. Lou, and J. Zhang. Preparation and friction behavior of carbon fiber reinforced silicon carbide matrix composites. *Ceramics International*, Vol. 33, No. 3, 2007 Apr, pp. 439–445.
- [124] Garshin, A. P., V. I. Kulik, and A. S. Nilov. Main areas for improving refractory fiber-reinforced ceramic matrix composite corrosion and heat resistance. *Refractories and Industrial Ceramics*, Vol. 58, 2018 Mar, pp. 673–682.
- [125] Hrubovčáková, M., T. Csanádi, R. Sedlák, A. Kovalčíková, I. Shepa, E. Múdra, et al. The effect of SiC whiskers addition on the microstructure and mechanical properties of a (Hf-Ta-Zr-Nb-Ti) C-SiC composite. *Ceramics International*, Vol. 49, No. 14, 2023 Jul, pp. 24179–24186.
- [126] Li, Z., R. Guo, L. Li, R. Zheng, and C. Ma. Microstructure and fracture toughness of SiAlCN ceramics toughened by SiCw or GNPs. *Ceramics International*, Vol. 49, No. 18, 2023 Sep, pp. 29709–29718.
- [127] Xue, R., P. Liu, Z. Zhang, N. Zhang, Y. Zhang, and J. Wang. Improvement of toughness of reaction bonded silicon carbide composites reinforced by surface-modified SiC whiskers. *Ceramics International*, Vol. 47, No. 13, 2021 Jul, pp. 18150–18156.
- [128] Xing, H., B. Zou, X. Wang, Y. Hu, C. Huang, and K. Xue. Fabrication and characterization of SiC whiskers toughened Al2O3 paste for stereolithography 3D printing applications. *Journal of Alloys and Compounds*, Vol. 828, 2020 Jul, id. 154347.
- [129] Yang, J., R. Yu, X. Li, Y. He, L. Wang, W. Huang, et al. Silicon carbide whiskers reinforced SiOC ceramics through digital light processing 3D printing technology. *Ceramics International*, Vol. 47, No. 13, 2021 Jul, pp. 18314–18322.
- [130] Zhu, T., W. Guo, J. Zhang, S. Sang, Y. Li, Z. Xie, et al. Synergistic toughening effect of SiC whiskers and particles in ZrO2-Al2O3-SiC ceramics. *Ceramics International*, Vol. 49, No. 22, 2023 Nov, pp. 36337–36343.
- [131] Fu, Q., S. Sui, Y. Ma, S. Sun, X. Wang, Q. Meng, et al. Silicon carbide whiskers reinforced silicon carbide ceramics prepared by vat photopolymerization and liquid silicon infiltration. *Ceramics International*, Vol. 50, No. 10, 2024 May, pp. 17747–17755.
- [132] Zhu, N., L. Zhang, G. Wen, and Y. Hou. Effect of SiC whiskers on the mechanical properties of polymer-derived ceramics prepared by digital light processing and its strengthening and toughening mechanism. *Journal of Alloys and Compounds*, Vol. 968, 2023 Dec, id. 171852.
- [133] Yang, Y., T. Zhu, N. Sun, X. Liang, Y. Li, H. Wang, et al. Mechanical and tribological properties of SiC whisker-reinforced SiC composites via oscillatory pressure sintering. *International Journal of Applied Ceramic Technology*, Vol. 20, No. 4, 2023 Jul, pp. 2499–2510.
- [134] Tiegs, T. SiC whisker reinforced alumina. *Handbook of ceramic composites*, Springer US, Boston, MA, 2005, pp. 307–323.
- [135] Garnier, V., G. Fantozzi, D. Nguyen, J. Dubois, and G. Thollet. Influence of SiC whisker morphology and nature of SiC/Al2O3 interface on thermomechanical properties of SiC reinforced Al2O3 composites. *Journal of the European Ceramic Society*, Vol. 25, No. 15, 2005 Oct, pp. 3485–3493.
- [136] Song, N., H. B. Zhang, H. Liu, and J. Z. Fang. Effects of SiC whiskers on the mechanical properties and microstructure of SiC ceramics

- by reactive sintering. *Ceramics International*, Vol. 43, No. 9, 2017 Jun, pp. 6786–6790.
- [137] Chen, N., L. Cheng, Y. Liu, F. Ye, M. Li, Z. Gao, et al. Microstructure and properties of SiCw/SiC composites prepared by gel-casting combined with precursor infiltration and pyrolysis. *Ceramics International*, Vol. 44, No. 1, 2018 Jan, pp. 969–979.
- [138] Wu, P., Y. Zheng, Y. Zhao, and H. Yu. Effect of SiC whisker addition on the microstructures and mechanical properties of Ti (C, N)based cermets. *Materials & Design*, Vol. 32, No. 2, 2011 Feb, pp. 951–956.
- [139] Zhou, H., J. Zhou, G. Liu, and H. Chen. Mechanical properties and wear properties of Si3N4/MoSi2/SiCw composite ceramic tool materials. *Journal of Functional Materials/Gongneng Cailiao*, Vol. 53, No. 10. 2022 Oct.
- [140] Wu, J., J. Li, and Y. Huang. Designing factors and fabricating technologies of ceramic matrix composite toughened by whisker. *Journal of the Chinese Ceramic Society*, Vol. 18, No. 1, 1990, pp. 72–82.
- [141] Becher, P. F., C. H. Hsueh, P. Angelini, and T. N. Tiegs. Toughening behavior in whisker-reinforced ceramic matrix composites. *Journal of the American Ceramic Society*, Vol. 71, No. 12, 1988 Dec, pp. 1050–1061.
- [142] Evans, A. G. Perspective on the development of high-toughness ceramics. *Journal of the American Ceramic society*, Vol. 73, No. 2, 1990 Feb, pp. 187–206.
- [143] Hu, J., R. S. Luo, C. K. Yao, and L. C. Zhao. Effect of annealing treatment on the stress corrosion cracking behavior of SiC whisker reinforced aluminum composite. *Materials chemistry and physics*, Vol. 70, No. 2, 2001 May, pp. 160–163.
- [144] Fei, W. D., M. Hu, and C. K. Yao. Thermal expansion and thermal mismatch stress relaxation behaviors of SiC whisker reinforced aluminum composite. *Materials chemistry and physics*, Vol. 77, No. 3, 2003 Jan, pp. 882–888.
- [145] Campbell, G. H., M. Rühle, B. J. Dalgleish, and A. G. Evans. Whisker toughening: a comparison between aluminum oxide and silicon nitride toughened with silicon carbide. *Journal of the American Ceramic Society*, Vol. 73, No. 3, 1990 Mar, pp. 521–530.
- [146] Homeny, J., W. L. Vaughn, and M. K. Ferber. Silicon carbide whisker/alumina matrix composites: effect of whisker surface treatment on fracture toughness. *Journal of the American Ceramic Society*, Vol. 73, No. 2, 1990 Feb, pp. 394–402.
- [147] Adalarasan, R., P. C. Shanmuga, R. Amnachalam, and R. Sudhir. An evaluation of mechanical properties and microstructure of dispersion strengthened Al-6063 obtained by in situ fabrication. International Journal on Design and Manufacturing Technologies, Vol. 5, No. 2, 2011.
- [148] Parikh, V. K., A. D. Badgujar, and N. D. Ghetiya. Joining of metal matrix composites using friction stir welding: a review. *Materials and Manufacturing Processes*, Vol. 34, No. 2, 2019 Jan, pp. 123–146.
- [149] Guo, H. and S. Zhang. Composite electroplating technology. 2007.
- [150] Yu, H. Metal matrix composite materials and their preparation techniques. 2006.
- [151] Yang, C., Z. Zhao, P. Bai, W. Du, and S. Zhang. Nano-SiC whisker-reinforced Ti6Al4V matrix composites manufactured by selective laser melting: fine equiaxed grain formation mechanism and mechanical properties. *Journal of Materials Processing Technology*, Vol. 317, 2023 Aug, id. 117981.
- [152] Qiu, H., X. Ban, and J. Liu. Effect of SiC whisker content on properties of magnesium matrix composite materials. *Powder Metallurgy Industry*, Vol. 26, No. 3, 2016, pp. 34–37.

- [153] Yan, D., G. Xu, Z. Yao, H. Liu, and Y. Chen. Synergistic Effect of Sic Particles and Whiskers on the Microstructures and Mechanical Properties of Ti (C, N)-Based Cermets. *Materials*, Vol. 15, No. 6, 2022 Mar, id. 2080.
- [154] Xu, Z., X. Shi, W. Zhai, Y. Wang, and S. Zhang. Fabrication and properties of tungsten-copper alloy reinforced by titaniumcoated silicon carbide whiskers. *Journal of Composite Materials*, Vol. 49, No. 13, 2015 Jun, pp. 1589–1597.
- [155] Wang, Y., M. Tayyebi, M. Tayebi, M. Yarigarravesh, S. Liu, and H. Zhang. Effect of whisker alignment on microstructure, mechanical and thermal properties of Mg-SiCw/Cu composite fabricated by a combination of casting and severe plastic deformation (SPD). *Journal of Magnesium and Alloys*, Vol. 11, No. 3, 2023 Mar, pp. 966–980.
- [156] Zhang, Y., L. Lai, D. Cui, Y. Zhu, H. Cai, B. Yan, et al. Hybrid effect on mechanical and thermal performance of copper matrix composites reinforced with SiC whiskers. *Ceramics International*, Vol. 50, No. 9, 2024 May, pp. 16553–16563.
- [157] Liu, S., Y. Wang, M. Yarigarravesh, M. Tayyebi, and M. Tayebi. Evaluation of whisker alignment and anisotropic mechanical properties of ZK60 alloy reinforced with SiCw during KOBO extrusion method. *Journal of Manufacturing Processes*, Vol. 84, 2022 Dec, pp. 344–356.
- [158] Han, L., J. Wang, S. Guo, Y. Chen, C. Shi, Y. Huang, et al. Fabrication and performance of SiC-reinforced Cu: Role of the aspect ratio of the SiC reinforcement phase. *Materials & Design*, Vol. 220, 2022 Aug, id. 110869.
- [159] Lianxi, H. and W. Erde. Fabrication and mechanical properties of SiCw/ZK51A magnesium matrix composite by two-step squeeze casting. *Materials Science and Engineering: A*, Vol. 278, No. 1–2, 2000 Feb, pp. 267–271.
- [160] Tayebi, M., S. Nategh, H. Najafi, and A. Khodabandeh. Tensile properties and microstructure of ZK60/SiCw composite after extrusion and aging. *Journal of Alloys and Compounds*, Vol. 830, 2020 Jul, id. 154709.
- [161] Gorsse, S. and D. B. Miracle. Mechanical properties of Ti-6Al-4V/ TiB composites with randomly oriented and aligned TiB reinforcements. *Acta Materialia*, Vol. 51, No. 9, 2003 May, pp. 2427–2442.
- [162] Peng, H. X. A review of "Consolidation effects on tensile properties of an elemental Al matrix composite" [Mater. Sci. Eng. A386 (2004) 194–204]. Materials Science and Engineering: A, Vol. 396, No. 1–2, 2005 Apr, pp. 1–2.
- [163] Yih, P. and D. D. Chung. Silicon carbide whisker copper-matrix composites fabricated by hot pressing copper coated whiskers. *Journal of Materials Science*, Vol. 31, 1996 Jan, pp. 399–406.
- [164] Li, M., F. Chen, X. Si, J. Wang, S. Du, and Q. Huang. Copper–SiC whiskers composites with interface optimized by Ti 3 SiC 2. *Journal* of *Materials Science*, Vol. 53, 2018 Jul, pp. 9806–9815.
- [165] Feng, J., S. Liang, X. Guo, Y. Zhang, and K. Song. Electrical conductivity anisotropy of copper matrix composites reinforced with SiC whiskers. *Nanotechnology Reviews*, Vol. 8, No. 1, 2019 Nov, pp. 285–292.
- [166] Faber, K. T. Ceramic composite interfaces: properties and design. Annual review of materials science, Vol. 27, No. 1, 1997 Aug, pp. 499–524.
- [167] Kindl, B., Y. L. Liu, E. Nyberg, and N. Hansen. The control of interface and microstructure of SiC/Al composites by sol-gel techniques. *Composites Science and technology*, Vol. 43, No. 1, 1992 Jan, pp. 85–93.

28

- [168] Lai, S. W. and D. D. Chung. Consumption of SiC whiskers by the Al–SiC reaction in aluminium-matrix SiC whisker composites. *Journal of Materials Chemistry*, Vol. 6, No. 3, 1996 Jan, pp. 469–477.
- [169] Tan, S. J., X. X. Zeng, Q. Ma, X. W. Wu, and Y. G. Guo. Recent advancements in polymer-based composite electrolytes for rechargeable lithium batteries. *Electrochemical Energy Reviews*, Vol. 1, 2018 Jun, pp. 113–138.
- [170] Banno, H. and K. Ogura. Dielectric and piezoelectric properties of a flexible composite consisting of polymer and mixed ceramic powder of PZT and PbTiO3. Ferroelectrics, Vol. 95, No. 1, 1989 Jul, pp. 171–174.
- [171] Kuo, D. H., C. C. Chang, T. Y. Su, W. K. Wang, and B. Y. Lin. Dielectric behaviours of multi-doped BaTiO3/epoxy composites. *Journal of the European Ceramic Society*, Vol. 21, No. 9, 2001 Sep, pp. 1171–1177.
- [172] Sakamoto, W. K., S. Kagesawa, D. H. Kanda, and D. K. Das-Gupta. Electrical properties of a composite of polyurethane and ferroelectric ceramics. *Journal of Materials Science*, Vol. 33, 1998 Jul, pp. 3325–3329.
- [173] Xu, J., X. Lei, D. Han, G. Liu, T. Yu, and M. Xing. Preparation and Dielectric Properties of Silane Coupling Agent Modified SiC Whisker/PVDF Composite Membrane. *Bulletin of the Chinese Ceramic Society*, Vol. 37, No. 9, 2018, pp. 3028–3035.
- [174] Zhou, W., X. Li, F. Zhang, C. Zhang, Z. Li, F. Chen, et al. Concurrently enhanced dielectric properties and thermal conductivity in PVDF composites with core-shell structured β-SiCw@ SiO₂ whiskers. *Composites Part A: Applied Science and Manufacturing*, Vol. 137, 2020 Oct. id. 106021.
- [175] Yu, T., W. Song, J. Feng, X. Peng, and W. Song. Research on thermal conductivity and insulation of oriented silicon carbide whisker silicone rubber composites. *Acta Materiae Compositae Sinica*, Vol. 41, No. 1, 2024 Jan.
- [176] Chen, J. P., Z. F. Wang, Z. L. Yi, L. J. Xie, Z. Liu, S. C. Zhang, et al. SiC whiskers nucleated on rGO and its potential role in thermal conductivity and electronic insulation. *Chemical Engineering Journal*, Vol. 423, 2021 Nov, id. 130181.
- [177] Liu, M. and D. Xiang. A low-cost approach for fabricating thermally conductive SiC/polymer composites by pre-constructing

- ceramic skeleton from photovoltaic silicon waste. *Sustainable Materials and Technologies*, Vol. 38, 2023 Dec, id. e00761.
- [178] Han, Y., X. Shi, S. Wang, K. Ruan, C. Lu, Y. Guo, et al. Nest-like hetero-structured BNNS@ SiCnws fillers and significant improvement on thermal conductivities of epoxy composites. *Composites Part B: Engineering*, Vol. 210, 2021 Apr, id. 108666.
- [179] Qin, Y., B. Wang, X. Hou, L. Li, C. Guan, Z. Pan, et al. Constructing Tanghulu-like Diamond@ Silicon carbide nanowires for enhanced thermal conductivity of polymer composite. *Composites Communications*, Vol. 29, 2022 Jan, id. 101008.
- [180] Cao, D., W. Zhou, M. Zhang, G. Cao, Y. Yang, G. Wang, et al. Insights into synchronously enhanced dielectric properties and thermal conductivity of β-SiCw/PVDF nanocomposites by building a crystalline SiO₂ shell as an interlayer. *Industrial & Engineering Chemistry Research*, Vol. 61, No. 23, 2022 May, pp. 8043–8056.
- [181] Dang, J., R. Wang, L. Yang, L. Gao, Z. Zhang, and M. Zha. Preparation of β-SiCw/BDM/DBA composites with excellent comprehensive properties. *Polymer Composites*, Vol. 35, No. 10, 2014 Oct, pp. 1875–1878.
- [182] Liu, Y., Y. Sun, Y. Wang, G. Ding, B. Sun, and X. Zhao. A complex reinforced polymer interposer with ordered Ni grid and SiC nanowhiskers polyimide composite based on micromachining technology. *Electronic Materials Letters*, Vol. 13, 2017 Jan, pp. 29–36.
- [183] Yang, Y., L. Lai, G. Ding, and T. Chen. SiC nanowire-based SU-8 with enhanced mechanical properties for MEMS structural layer design. *Nanotechnology and Precision Engineering*, Vol. 2, No. 4, 2019 Dec, pp. 169–176.
- [184] Zhang, N., A. Yu, A. Liang, R. Zhang, F. Xue, and E. Ding. Preparation of SiC whisker and application in reinforce of polystyrene resin composite materials. *Journal of Applied Polymer Science*, Vol. 130, No. 1, 2013 Oct, pp. 579–586.
- [185] Pan, L. Research on preparation and properties of polyurethane bonding SiC particles composites. *Master's thesis*, Xi'an University of Technology.
- [186] Hui, Y., Z. Ling-Jie, G. Xing-Zhong, Z. Lin, and S. Jian-Chao. Dispersion Behavior of SiC Micro Whiskers in Aqueous Medium. *Chinese Journal* of *Inorganic Chemistry*, Vol. 28, No. 1, 2012 Jan, pp. 153–158.